Rathke's cleft-like cysts arise from *Isl1* deletion in murine pituitary progenitors

Michelle L. Brinkmeier,[1] Hironori Bando,[1] Adriana C. Camarano,[2] Shingo Fujio,[3] Koji Yoshimoto,[3] Flávio S.J. de Souza,[2] and Sally A. Camper[1]

[1]Department of Human Genetics, University of Michigan Medical School, Ann Arbor, Michigan, USA. [2]Institute of Physiology, Molecular Biology, and Neurosciences-IFIBYNE-CONICET, Pabellon IFIBYNE, Ciudad Universitaria, Buenos Aires, Argentina. [3]Graduate School of Medical and Dental Sciences, Department of Neurosurgery, Kagoshima University, Kagoshima, Japan.

The transcription factor ISL1 is expressed in pituitary gland stem cells and the thyrotrope and gonadotrope lineages. Pituitary-specific *Isl1* deletion causes hypopituitarism with increased stem cell apoptosis, reduced differentiation of thyrotropes and gonadotropes, and reduced body size. Conditional *Isl1* deletion causes development of multiple Rathke's cleft-like cysts, with 100% penetrance. *Foxa1* and *Foxj1* are abnormally expressed in the pituitary gland and associated with a ciliogenic gene-expression program in the cysts. We confirmed expression of FOXA1, FOXJ1, and stem cell markers in human Rathke's cleft cyst tissue, but not craniopharyngiomas, which suggests these transcription factors are useful, pathological markers for diagnosis of Rathke's cleft cysts. These studies support a model whereby expression of ISL1 in pituitary progenitors drives differentiation into thyrotropes and gonadotropes and without it, activation of FOXA1 and FOXJ1 permits development of an oral epithelial cell fate with mucinous cysts. This pituitary-specific *Isl1* mouse knockout sheds light on the etiology of Rathke's cleft cysts and the role of ISL1 in normal pituitary development.

Introduction

The pituitary gland forms from an evagination of neural ectoderm that forms the posterior lobe and an invagination of oral ectoderm called Rathke's pouch, which gives rise to the anterior and intermediate lobes. A residual cleft remains at the junction between the anterior and intermediate lobes in rodents, although this normally regresses and is less distinct in humans. The cells lining the cleft are thought to be the origin of various cystic lesions, including Rathke's cleft cysts (RCC), epidermoid, cysts and craniopharyngiomas (reviewed in refs. 1–4). RCCs are common, benign lesions that can become enlarged and cause headache, visual disturbances, pituitary dysfunction, pituitary apoplexy, and/or diabetes insipidus.

RCCs are frequently asymptomatic and identified incidentally by head-imaging studies. In these cases, imaging may be repeated periodically to monitor cyst growth. Symptomatic cysts are typically treated by transsphenoidal surgery to drain and/or resect the cyst (5, 6). The most common complication is postoperative diabetes insipidus, which occurs in direct correlation with the aggressiveness of cyst resection. Individuals requiring RCC surgery have an 18% recurrence rate within 5 years, and 57% of those require repeated surgeries.

RCCs are diagnosed with a combination of radiological and histopathological features. Most RCCs are within the region of the sella turcica between the anterior and posterior lobes, but some extend beyond the sella to the optic chiasm. RCCs are lined with ciliated cuboidal or columnar epithelial cells interspersed with goblet cells (7). There can be evidence of squamous metaplasia, hemorrhage, inflammation, and fibrosis (8). Histological overlap among RCCs, craniopharyngiomas, and epithelial cysts can confound diagnosis (9).

The origin of RCCs is not clear. There have been no systematic genetic studies to investigate pathology in humans. There are a few anecdotal reports of genetic lesions with complex phenotypes that include RCCs, but it is not clear whether those cysts are incidental, given the high rate of cystic lesions found in autopsy cases (33%) (10–12). Rodents can also spontaneously develop RCC-like lesions in the pars distalis and pars tuberalis, and the incidence is reported to range from approximately 1% to 10% (13, 14). Cysts are hypothesized to arise from oral ectoderm cells of the pharyngeal duct that fail to degenerate. This idea is supported by the ability of oral epithelium to form cystic structures when transplanted into the brain (15). Transgenic mouse models of cystic lesions were generated by driving very high levels of leukemia inhibitor factor (LIF) expression in the developing pituitary gland (16, 17). LIF is an IL-6 class cytokine that can either inhibit or promote cell differentiation, depending on the organ system (18). The relevance of the LIF transgenic models is not clear because LIF expression is not normally detected during mouse development and it is expressed in both RCC and craniopharyngiomas (19). Disruption of Hippo signaling during embryonic pituitary development leads to tumor development with characteristics of RCCs and squamous cell carcinomas (20, 21).

Transcription factors play important roles in driving organ development and cell fate. Several LIM homeodomain transcription factors are expressed early in pituitary development. Mouse knockouts of *Lhx2*, *Lhx3*, and *Lhx4* revealed the importance of each gene for pituitary development (22–27). *Lhx2* is important for development of the infundibulum and pituitary stalk, but it is not necessary for specification of hormone-producing cells in the

Conflict of interest: The authors have declared that no conflict of interest exists.

Submitted: January 27, 2020; **Accepted:** May 14, 2020; **Published:** July 20, 2020.
Reference information: *J Clin Invest*. 2020;130(8):4501–4515.
https://doi.org/10.1172/JCI136745.

anterior pituitary. *Lhx3* and *Lhx4* have overlapping and essential roles in expansion of Rathke's pouch and hormone cell specification. Loss-of-function mutations in the human *LHX3* and *LHX4* genes are associated with multiple pituitary hormone deficiencies. Less is known about the role of the LIM homeodomain transcription factor ISL1 in pituitary development.

ISL1 was discovered through its ability to bind essential cis-acting sequences of the rat insulin gene, and it is required for the development of all pancreatic endocrine cells (28, 29). ISL1 is also an important cell-fate regulator in the development of the heart, eye, ear, motor neurons, cholinergic neurons, hypothalamus, tooth, hind limb, and pylorus (30–38). In the pituitary gland, *Isl1* is initially expressed throughout the region of oral ectoderm that will become Rathke's pouch (E9.5–E10.5), preceding *Lhx3* and *Lhx4* expression (39–41). It becomes localized to the differentiating cells at the ventral aspect of the organ (E11.5), and it is specific for thyrotropes and gonadotropes (E16.5–P7) (42). *Isl1* transcripts are greatly elevated in a mouse model of thyrotrope hypertrophy (43). Based on the expression pattern in developing pituitary gland and the role of *Isl1* in development of other organs, we hypothesized that *Isl1* could play an important role in cell specification of the pituitary gland. Embryos with a targeted deletion in *Isl1* die by E10 due to heart defects, and only a thin, rudimentary Rathke's pouch is formed (38, 41). Conditional deletion of *Isl1* in committed thyrotropes using *Tshb-cre* produced modest growth insufficiency, mild hypothyroidism, and a reduced pituitary response to a hypothyroid challenge (42).

Here, we report that deletion of *Isl1* in the pituitary gland before cell specification has 3 major effects: (a) Rathke's pouch dysmorphology with modestly reduced growth, (b) substantially reduced differentiation of progenitors into thyrotropes and gonadotropes, and (c) development of multiple Rathke's cleft-like cysts (RCC-like). We analyzed the molecular pathogenesis of cyst formation and discovered that abnormal expression of the pioneer transcription factor FOXA1 appears to drive expression of FOXJ1 and ciliogenic and mucinous cell fates. This embryonic analysis of RCC-like development accurately predicted markers that distinguish human RCC (hRCC) from craniopharyngiomas. Thus, *Isl1* has an important role in driving pituitary organogenesis and suppressing the differentiation of oral ectoderm into alternate cell fates.

Results

ISL1 is expressed in pituitary progenitor cells, consistent with a role in cell-fate choices. ISL1 is expressed at E8.5–E9.5 in the oral ectoderm that will become Rathke's pouch, and it becomes localized to thyrotropes and gonadotropes (39, 42). At E10.5 and E11.5, ISL1 expression was strongest in the ventral aspect of Rathke's pouch, and it extended slightly beyond the point of separation between Rathke's pouch and the underlying oral ectoderm (Figure 1, A and B). At E16.5, the pattern of ISL1 expression in scattered cells in the anterior lobe was consistent with previous reports of enrichment in developing thyrotropes and gonadotropes (Figure 1C). At this time, little or no ISL1 expression was detected in the marginal zone, located along the cleft between the intermediate and anterior lobes of the pituitary. After birth, at P3 and P7, ISL1 was clearly expressed in the cells within the marginal zone (Figure 1D). Stem cells that can self-renew and give rise to all hormone-producing cell types are marked by SOX2 and PROP1, and they reside in the marginal zone and in small clusters within the parenchyma of the anterior lobe (44–47). *Prop1* and *Sox2* expression largely coincided at E12.5, but *Prop1* was enriched in the cells transitioning to differentiate at E14.5. Postnatally, many ISL1-positive cells coexpressed PROP1 and SOX2 in the marginal zone and the parenchyma (Figure 1, E and F). The temporal and spatial expression pattern of ISL1 was consistent, with the potential to regulate pituitary stem cells and cell specification.

Deletion of Isl1 affects growth and morphology of Rathke's pouch and causes cyst formation. To assess the role of ISL1 in the pituitary progenitor cells after definitive Rathke's pouch formation, we selected the *Prop1-cre* transgenic line for conditional deletion of *Isl1* (48, 49). The *Prop1-cre* line genetically labels a few pituitary cells at E11.5 and completely labels cells in the anterior and intermediate lobes by E12.5. *Prop1-cre; Isl1*$^{+/-}$ mice were mated with *Isl1*$^{fl/fl}$ mice, and embryos were collected at various times. To assess the efficiency of *Prop1-cre*–mediated *Isl1* deletion, we used PCR analysis of genomic DNA isolated from pituitary glands at birth (Supplemental Figure 1A; supplemental material available online with this article; https://doi.org/10.1172/JCI136745DS1). Only the null allele of *Isl1* was evident in *Prop1-cre; Isl1*$^{fl/-}$ samples. The floxed allele was not detectable, indicating efficient deletion of *Isl1*. We also conducted immunostaining for ISL1 at E11.5, E16.5, and P3 (Supplemental Figure 1, B–F). Only a few ISL1-positive cells were detected at E11.5 and E16.5, and none were detected at P3. This confirmed the robust, efficient deletion of *Isl1* in *Prop1-cre; Isl1*$^{fl/-}$ mice, hereafter referred to as *Isl1*^{Prop1KO}.

Isl1^{Prop1KO} showed Rathke's pouch dysmorphology early in pituitary organogenesis (Figure 1, G–L). At E11.5, the mutant Rathke's pouch appeared smaller, and dysmorphic regions appeared on the pouch surface adjacent to the mesenchyme. It appeared as if progenitors were disorganized or were excluded from the pouch. At E13.5 and E14.5, the dysmorphology became more pronounced and was present at the outer edges of both the anterior and intermediate lobes. We examined the levels of proliferation and cell death at E11.5 and quantified the size of Rathke's pouch (Figure 1, M–Q). We analyzed proliferation by immunostaining with antibodies against cyclin D1 (CCND1), a cell cycle marker highly expressed in the G_1 phase. In control embryos, CCND1 was expressed in a gradient, with the highest level at the dorsal aspect of Rathke's pouch, and there was no expression at the ventral aspect where cells were beginning to undergo differentiation. *Isl1*^{Prop1KO} mutants expressed CCND1, and proliferating cells extended into the ventral region, indicating a loss of the expression gradient. Apoptosis, visualized by cleaved caspase-3 immunostaining, normally occurs at E11.5 in cells located where Rathke's pouch separates from the oral ectoderm. A few additional apoptotic cells were evident dorsally in *Isl1*^{Prop1KO} mutant pouches, indicating an increase in cell death. At E11.5, Rathke's pouch was approximately 22% smaller in the mutants than controls.

To determine whether earlier deletion of *Isl1* would have a more profound effect on the growth of Rathke's pouch, we used a *Hesx1-cre* line that drives cre activity in Rathke's pouch and some of the surrounding oral ectoderm at E10.5 (50). We confirmed reduced expression of ISL1 at E11.5 in *Hesx1-cre; Isl1*$^{fl/fl}$ mice (*Isl1*^{Hesx1KO}) (Supplemental Figure 1G). The *Isl1*^{Hesx1KO} embryos

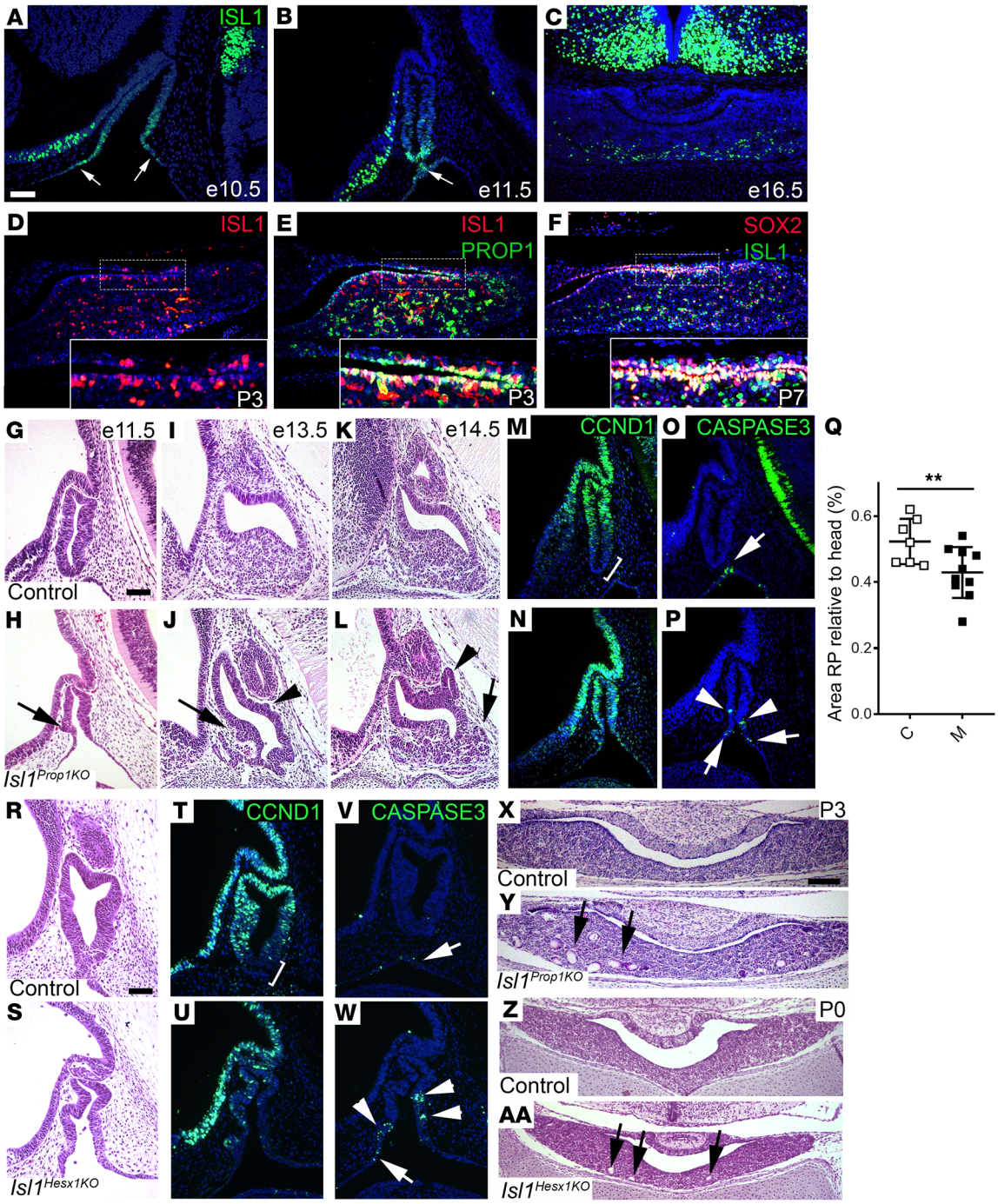

Figure 1. ISL1 expression in pituitary progenitor cells is important for growth and morphology. (**A**–**D**) ISL1 immunostaining reveals ventral expression in Rathke's pouch and oral epithelium at E10.5 (n = 2) and E11.5 (n = 7) (arrows), ventral expression at E16.5 (n = 2), and expression in the marginal zone and parenchyma at P3 (n = 3). (**E** and **F**) ISL1 costains with PROP1 at P3 (n = 2) and SOX2 at P7 (n = 2). Insets show marginal zone (**D**–**F**). (**G**–**L**) H&E staining from control and *Isl1*^{Prop1KO} pituitaries at E11.5 (control, n = 7; *Isl1*^{Prop1KO}, n = 10), E13.5 (control, n = 4; *Isl1*^{Prop1KO}, n = 4), and E14.5 (control, n = 3; *Isl1*^{Prop1KO}, n = 5) reveals dysmorphology in anterior (arrows) and intermediate lobes (arrowheads). (**M** and **N**) CCND1 immunostaining of control (n = 4) and *Isl1*^{Prop1KO} (n = 6) pituitaries at E11.5 (bracket denotes negative region). (**O** and **P**) Immunostaining for cleaved caspase-3 detected apoptotic cells in E11.5 control (n = 6) and *Isl1*^{Prop1KO} mutants (n = 13) at normal (arrows) and ectopic sites (arrowheads). (**Q**) Size of Rathke's pouch (RP) was normalized to head size and displayed as percentage. *Isl1*^{Prop1KO} (M, n = 10; range 0.28%–0.54%) was significantly smaller than controls (C, n = 7; range 0.45%–0.62%) based on Student's t test, 1-tail distribution, 2-sample unequal variance. $^{**}P < 0.01$. (**R** and **S**) H&E staining of control (n = 4) and *Isl1*^{Hesx1KO} (n = 4) pituitaries at E11.5 confirm dysmorphology. (**T**–**W**) CCDN1 (control, n = 2; *Isl1*^{Hesx1KO}, n = 3) and cleaved caspase-3 (control, n = 2; *Isl1*^{Hesx1KO}, n = 3) expression confirm abnormal growth. (**X** and **Y**) H&E staining of control (n = 3) and *Isl1*^{Prop1KO} pituitaries (n = 3) reveals multiple cysts at P3 in mutants (arrows). (**Z** and **AA**) H&E staining of control (n = 2) and *Isl1*^{Hesx1KO} pituitaries (n = 2) reveals cyst formation at P0 (arrows). Scale bars: 50 μm (**A**–**P**, **R**–**W**); 100 μm (**X**–**AA**). Original magnification, ×400 (insets).

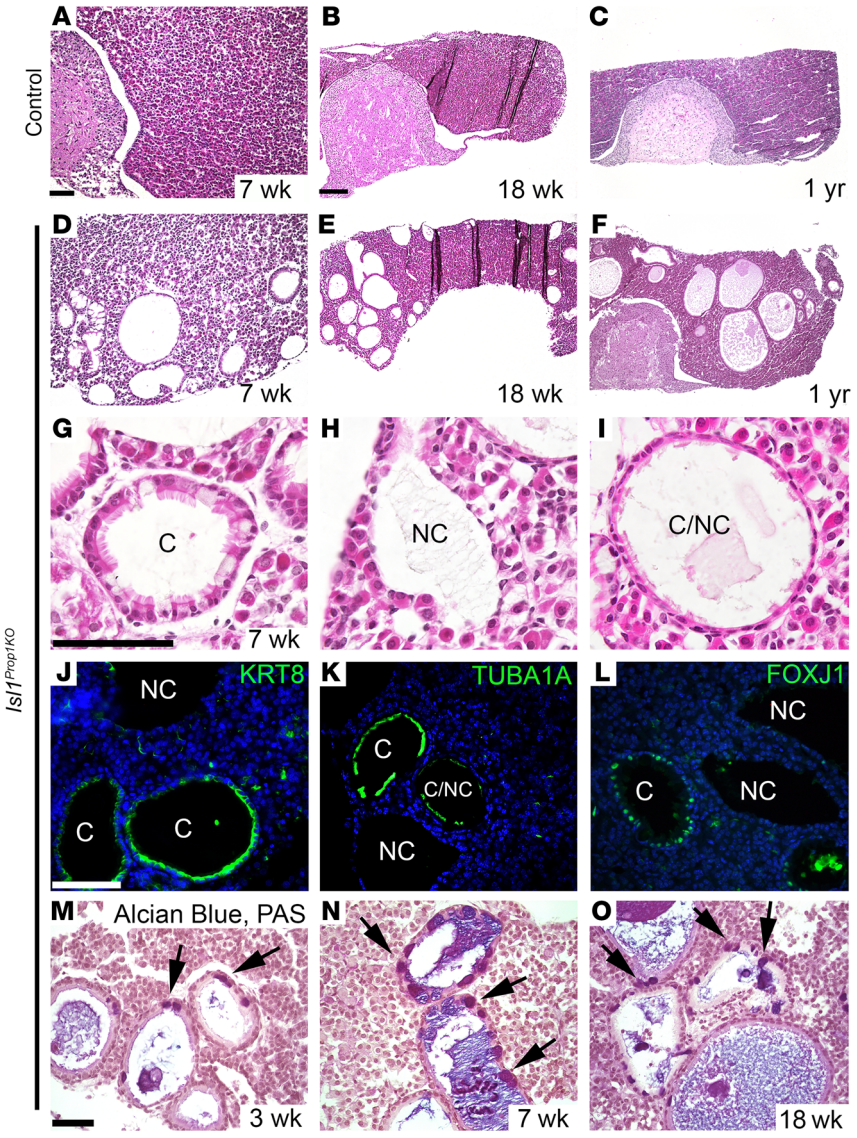

Figure 2. *Isl1*^{Prop1KO} cysts expand with age and have characteristics of hRCCs. (**A**–**I**) Pituitary gland sections from control and *Isl1*^{Prop1KO} mutants collected at 7 weeks (control, n = 4; *Isl1*^{Prop1KO}, n = 10), 18 weeks (control, n = 3; *Isl1*^{Prop1KO}, n = 4), and 1 year (control, n = 2; *Isl1*^{Prop1KO}, n = 2) were stained with H&E. Multiple cysts are evident throughout adulthood in *Isl1*^{Prop1KO} mutants. Cysts contain ciliated epithelium (C), nonciliated epithelium (NC), or a combination of ciliated and nonciliated epithelium (C/NC). (**J**–**L**) Immunostaining for cytokeratin 8 (KRT8), acetylated tubulin (TUBA1A), and FOXJ1 at 7 weeks detected expression of characteristic markers of hRCCs in *Isl1*^{Prop1KO} mutants (n = 3). (**M**–**O**) Alcian blue/PAS staining detects mucosal cell (arrows) lining within the cyst walls from weaning (3 weeks, n = 1) through adulthood (7 weeks, n = 7; 18 weeks, n = 3) in *Isl1*^{Prop1KO} mutants. Scale bars: 50 μm (**A**, **D**, **M**–**O**); 100 μm (**B**, **C**, **E**–**L**).

exhibited extensive dysmorphology, reduced CCND1 expression throughout the pouch, and larger patches of apoptotic cells (Figure 1, R–W) than *Isl1*^{Prop1ko} at the same time.

ISL1 deficiency is associated with cyst formation in pituitaries of *Isl1*^{Prop1KO} and *Isl1*^{Hesx1KO} mice. After birth, numerous cyst-like structures were present within the anterior lobe in *Isl1*^{Prop1KO} mutants (Figure 1, X and Y). No cysts were observed in association with the pituitary stalk. Of the *Isl1*^{Prop1KO} pituitary glands, 100% had multiple cysts. Multiple cysts were present in the *Isl1*^{Hesx1KO} mutant pituitaries at birth (Figure 1, Z and AA).

To identify the origin of the cells within the cysts, we conducted a lineage-tracing experiment using a *Rosa26* cre reporter strain that genetically labels cells with yellow fluorescent protein (YFP) (Supplemental Figure 1, H–J). *R26R-EYFP* homozygotes were crossed with *Isl1*$^{fl/fl}$ mice, and the progeny were bred to *Isl1*$^{fl/fl}$ mice to generate *Isl1*$^{fl/fl}$*; R26R*$^{EYFP/+}$ mice. The mice were crossed with *Prop1-cre; Isl1*$^{+/-}$ mice. Neonates were harvested and analyzed for YFP expression by immunohistochemistry. In *Isl1*^{Prop1KO}*; R26R*$^{EYFP/+}$ newborns, we detected YFP immunostaining in the majority of cells throughout the anterior and intermediate lobes of the pituitary gland, including the marginal zone where progenitors reside. The level of immunostaining varied, as reported in lineage-tracing studies for other tissues (51, 52). The cells lining the cysts were also YFP labeled, although the intensity range was less than for the hormone-producing cells. As expected, no YFP staining was observed in the blood vessels of the anterior pituitary gland, as these are derived from the neural crest, not the oral ectoderm (48). There was no background YFP immunoreactivity in the posterior lobe of the pituitary gland, brain, mesenchyme, or cartilage. There was also no background YFP immunoreactivity in the anterior or intermediate lobes of *Prop1-cre; Isl1*$^{+/fl}$ mice without the *R26R-EYFP* reporter. Thus, the cells lining the cysts are derived from the oral ectoderm of Rathke's pouch.

Isl1^{Prop1KO} *pituitaries have Rathke's cleft-like cysts*. We analyzed the cysts in the pituitaries of *Isl1*^{Prop1KO} mice at 7 weeks, 18 weeks, and 1 year using histology, immunochemistry, and standard pathological stains. The cysts increased in size and number as the mice aged, and multiple cysts were observed in 100% of the mutants (Figure 2, A–F). We identified 3 types of cysts in *Isl1*^{Prop1KO} mutant pituitaries (Figure 2, G–I). Some cysts were lined with cil-

Table 1. *Isl1*^{PROP1KO} mutant pituitaries express markers characteristic of RCCs

Gene family	Genes	Fold change
Mucinous secretion	Regenerating islet-derived 3g (*Reg3g*)	76×
	Mucin5, subtype b (*Muc5b*)	48×
Cytokeratins	Keratin 15 (*Krt15*)	37×
	Keratin 5 (*Krt5*)	31×
	Keratin 13 (*Krt13*)	14×
	Keratin 4 (*Krt4*)	7×
	Keratin 23 (*Krt23*)	4×
	Keratin 19 (*Krt19*)	4×
	Keratin 14 (*Krt14*)	3×
	Keratin 8 (*Krt8*)	2×
	Keratin 17 (*Krt17*)	2×
Cilia development	Apical cilia structure protein (*Sntn*)	26×
	Multiciliate differentiation and DNA synthesis (*Mcidas*)	20×
	Forkhead box J1 (*Foxj1*)	2.5×
Papillary craniopharyngioma	Braf transforming gene (*Braf*)	0.99×
Adamantinomatous craniopharyngioma	β-catenin (*Ctnnb1*)	1×
	Axin2 (*Axin2*)	1×
Cytokine	Leukemia inhibitory factor (*LIF*)	1×
Hippo pathway	Cysteine rich protein 61 (*Cyr6)1*	1×
	Connective tissue growth factor (*Ctgf*)	1×

iated epithelial cells interspersed with mucosal cells, some cysts were lined with squamous epithelial cells, and some were lined with a combination of the two. This is similar to reports of RCCs in human patients: cysts are lined with ciliated cuboidal or columnar epithelial cells with mucosal cells interspersed, or they are lined with squamous epithelial cells (53, 54). Cytokeratins are characteristic markers of hRCCs (55, 56), while craniopharyngiomas are marked by BRAF and members of the WNT signaling pathway (57–59). The forkhead transcription factor FOXJ1 is a marker of the ciliated cuboidal and columnar cells of hRCCs (60). The cells lining the cysts in *Isl1*^{Prop1KO} mutants were positive for cytokeratin 8, acetylated tubulin (a marker of cilia), and FOXJ1 (Figure 2, J–L). Mucosal cells were identified in the cyst walls by Alcian blue/periodic acid–Schiff (PAS) staining (Figure 2, M–O, and ref. 61).

RNA-Seq analysis was performed on whole pituitary glands from 6 P0 *Isl1*^{Prop1KO} mutants and 6 P0 controls. The quality and comparability of the individual mutant and control samples were characterized by principal component analysis. Approximately 74% of the variance could be explained by principal components 1 and 2, and differentially expressed genes segregated with the genotypes (Supplemental Figure 2). Analysis of transcriptional changes revealed increased expression of genes in *Isl1*^{Prop1KO} pituitaries that are associated with hRCCs, such as keratins and *Foxj1*, but not papillary (PCP) or adamantinomatous (ACP) craniopharyngiomas, including *Braf*, β-catenin, and *Axin2* (Table 1). Disruption of hippo signaling and overexpression of *Lif* are associated with cyst formation in mouse glands (16, 17, 20, 21). There was no change in expression of downstream targets of the hippo signaling pathway, *Cyr61* and *Ctgf*, or *Lif* in *Isl1*^{Prop1KO} pituitaries at birth.

ISL1 regulates early specification of gonadotrope and thyrotrope lineages. We hypothesized that ISL1 could have a role in the specification of gonadotrope and thyrotrope lineages because it is coexpressed with hormone markers of those lineages early in development (42). We used immunostaining to assess expression of pituitary transcription factors and hormones. LHX3 is an essential transcription factor for expansion of Rathke's pouch and most pituitary hormone-producing cells in mice and humans (62, 63). LHX3 immunostaining was normal in the *Isl1*^{Prop1KO} mutants at E12.5, indicating commitment to pituitary fate and normal establishment of a dorsal-to-ventral gradient of LHX3 expression (Supplemental Figure 3, A and B). FOXL2, an early transcription factor marker of gonadotropes and thyrotropes, was reduced in *Isl1*^{Prop1KO} mutants at E13.5 compared with controls, and the common hormone subunit CGA was nearly undetectable in mutants (Figure 3, A–D). At E16.5, fewer TSHβ immunopositive cells were detected in the caudomedial area, and none were detected in the POU1F1-independent rostral tip region (Figure 3, E and F). Immunostaining for the gonadotrope-specific transcription factor NR5A1 (SF1) revealed only a few positive cells in mutants at E16.5 (Figure 3, G and H). These data support the hypothesis that *Isl1* is necessary for promoting differentiation into gonadotropes and thyrotropes.

To investigate the specificity and mechanism of this effect, we examined expression of other lineage-specific transcription factors and hormone markers. POMC was properly expressed in the *Isl1*^{Prop1KO} mutants at E14.5, indicating normal commitment to the corticotrope lineage (Supplemental Figure 3, C and D). *Gata2* is an important transcription factor for thyrotropes and gonadotropes (64–67). In situ hybridization revealed comparable levels of *Gata2* transcripts in both the rostral tip and caudo-medial area of control and *Isl1*^{Prop1KO} mutant pituitary glands (Figure 3, I and J). POU1F1, the signature transcription factor for the somatotrope, lactotrope, and thyrotrope lineages, was also similarly expressed in the *Isl1*^{Prop1KO} mutants (Supplemental Figure 3, E and F). Taken together, these data suggest that ISL1 deficiency caused reduced commitment to thyrotrope and gonadotrope lineages by influencing expression of *Foxl2* and *Nr5a1* without affecting expression of *Gata2* or *Pou1f1* or commitment to corticotrope fate.

We conducted cell counts and RNA-Seq analysis in newborn pituitary glands to quantify the effect of *Isl1* deficiency and to determine whether reduced lineage-specific commitment could be attributed to developmental delay. The numbers of gonadotrope and thyrotrope cells were reduced in P3 *Isl1*^{Prop1KO} neonates. Immunoreactive LHβ and TSHβ cells were reduced 3-fold and 1.9-fold, respectively (Figure 3, K–P). RNA-Seq analysis revealed that transcripts for *Cga*, which encodes the common α-subunit of the gonadotropins and thyrotropin, were reduced to 0.2 times the levels in normal mice (Table 2). Transcripts for gonadotrope markers gonadotropin-releasing hormone receptor gene (*Gnrhr*), *Lhb*, and *Fshb* were reduced to 0.12–0.2 times. Transcripts for *Nr5a1* and *Foxl2* were reduced 0.4–0.54 times. Thyrotrope-specific markers *Rgs4*, *Tshr*, *Dio2*, and *Tshb* were reduced 0.52–0.66 times. Markers of progenitors and other pituitary lineages were unchanged, including the corticotrope and melanotrope markers *Tbx19* and *Pomc*, the somatotrope markers *Gh* and *Ghrhr*, and the markers of the somatotrope, lactotrope, and thyrotrope progenitors *Prop1* and

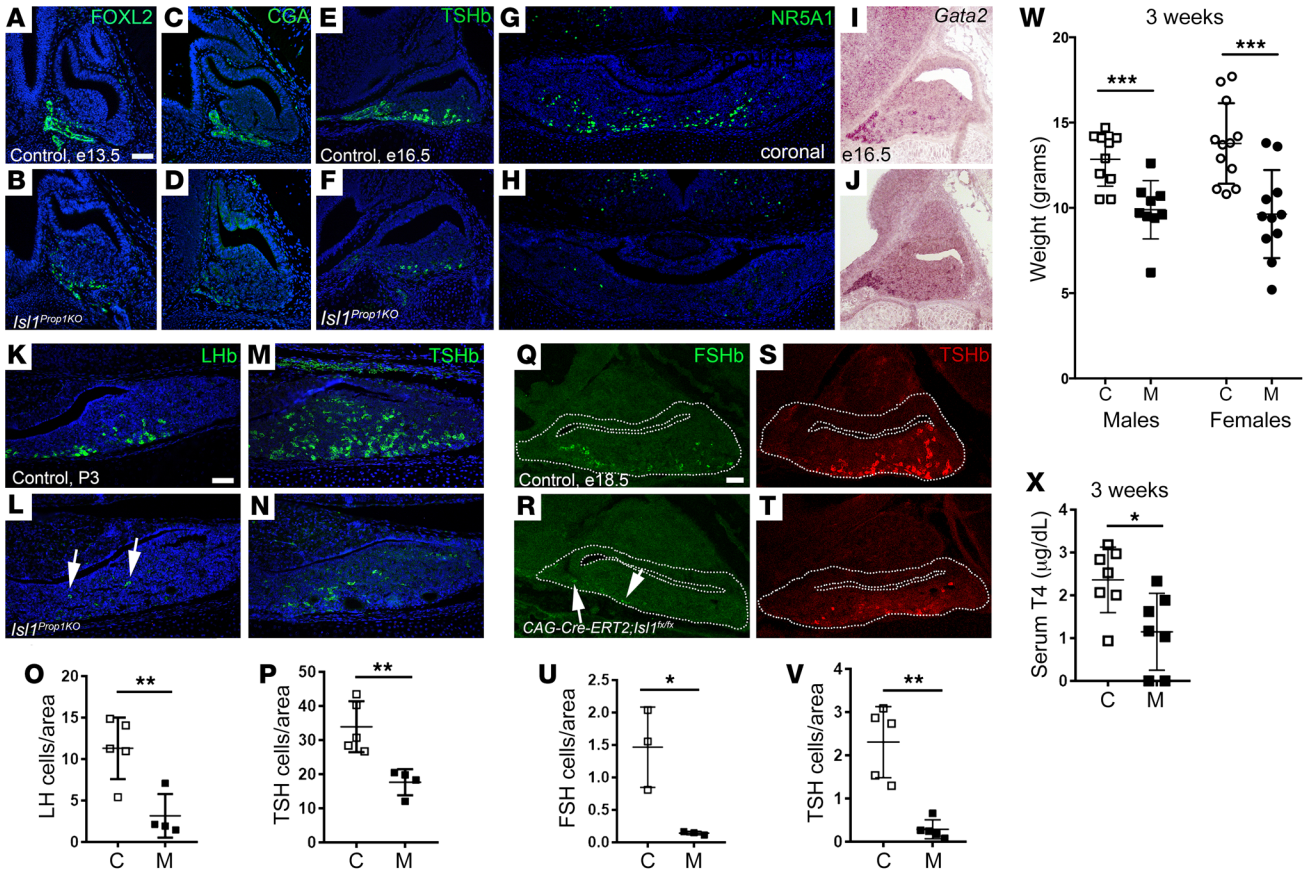

Figure 3. *Isl1* is required for gonadotrope and thyrotrope lineages. (**A**–**D**) FOXL2 and CGA immunostaining in control (**A**, $n = 3$; **C**, $n = 4$) and $Isl1^{Prop1KO}$ (**B**, $n = 3$; **D**, $n = 4$) pituitary glands at E13.5. (**E** and **F**) TSH immunostaining in control ($n = 3$) and $Isl1^{Prop1KO}$ ($n = 7$) pituitary glands at E16.5.(**G** and **H**) NR5A1 immunostaining in E16.5 control ($n = 3$) and $Isl1^{Prop1KO}$ ($n = 3$) pituitaries. (**I** and **J**) Gata2 ISH in E16.5 pituitaries of control ($n = 7$) and $Isl1^{Prop1KO}$ ($n = 8$). (**K**–**N**) LH and TSH immunostaining in P3 pituitaries in controls ($n = 3$) and $Isl1^{Prop1KO}$ ($n = 3$). (**O** and **P**) Quantitation of LH and TSH immunopositive cells per unit area of the pituitary at P0 reveals decreases in gonadotropes (control, $n = 5$, range = 5.4–14.9; $Isl1^{Prop1KO}$, $n = 4$, range = 1.5–7.1) and thyrotropes (control, $n = 5$, range = 26.7–43.4; $Isl1^{Prop1KO}$, $n = 4$, range = 12.1–20.5) in $Isl1^{Prop1KO}$. (**Q**–**T**) E18.5 control and tamoxifen-induced ablation of ISL1 (*CAG-Cre-ERT2;*$Isl1^{fl/fl}$) mouse model were immunostained for FSH (control, $n = 3$; mutant, $n = 3$) and TSH (control, $n = 5$; mutant, $n = 5$). Arrows indicate rare gonadotropes in both types of ISL1-deficient mutants. (**U** and **V**) Quantitation of FSH- and TSH-positive cells per unit area revealed decreases in both cell populations in *CAG-Cre-ERT2;*$Isl1^{fl/fl}$ mutants (FSH, range = 0.14–0.2; TSH, range = 0.2–0.7) relative to controls (FSH, range = 0.8–2.0; TSH, range = 1.3–3.1). (**W**) Male and female $Isl1^{Prop1KO}$ mice (male, $n = 8$, range = 6.2–12.6 g; female, $n = 11$, range = 5.2–13.8g) weigh less than control littermates (male, $n = 10$, range = 10.5–14.7 g; female, $n = 12$, range = 10.8–17.7 g) at 3 weeks and have reduced serum T4 (**X**, control, $n = 7$, range = 0.94–3.18; mutant, $n = 7$, range = 0.0–2.33). Scale bars: 50 μm (**A**–**L**, **N**, **O**, **Q**–**U**). Sagittal orientation (**A**–**F**, **I**, **J**, **Q**–**U**), coronal orientation (**G**, **H**, **K**–**O**). Statistical significance was determined using Student's *t* test, 1-tail distribution, 2-sample equal variance (**O**, **P**, and **U**–**X**). $^*P < 0.05$; $^{**}P < 0.01$; $^{***}P < 0.001$.

Pou1f1. These data document a quantitative, persistent, and specific diminution of gonadotropes and thyrotropes.

To determine whether *Isl1* deletion by other methods would produce similar results, we deleted *Isl1* using a tamoxifen-inducible cre recombinase system and *Hesx1-cre*. *CAG-Cre-ER*^{T2} mice (68) were mated to $Isl1^{fl/fl}$ animals to generate *CAG-Cre-ER*^{T2}*;* $Isl1^{fl/fl}$ male mice, which were then mated to $Isl1^{fl/fl}$ females. Pregnant females were injected with tamoxifen at E12.5, and embryos were harvested at E18.5. Analysis of gonadotrope and thyrotrope specification revealed a 10-fold reduction in FSHβ immunoreactive cells and a 7.5-fold reduction in TSHβ immunoreactive cells compared with those of control littermates (Figure 3, Q–V). The specification of corticotropes was unchanged (Supplemental Figure 3, G–I). Consistent with this, $Isl1^{Hesx1KO}$ mutants also had a reduction in TSH and LH immunostaining (Supplemental Figure 3, J–O). The reduction in thyrotrope and gonadotrope differentiation was variable and tended to be milder than in the other *Isl1* deletion models, probably because a significant number of ISL1 immunopositive cells were detectable in newborn $Isl1^{Hesx1KO}$ pituitaries, consistent with less efficient deletion in this model.

We examined the genotype distribution and the physiological consequence of reduced *Isl1* deficiency at various ages in the $Isl1^{Prop1KO}$ mutants. The survival rate was reduced: only 8% of the newborn progeny were mutants instead of the expected 25% (Supplemental Figure 3P). At weaning, surviving male and female mutants had a 23% and a 30% reduction in body weight, respectively (Figure 3W), which is consistent with the persistent reduction in thyrotropes. By 7 weeks, mutant females only exhibited a 12% reduction in body weight, and mutant males were not significantly different from controls (Supplemental Figure 3Q). Free serum T4 levels were reduced in $Isl1^{Prop1KO}$ mutants at weaning, and TSHβ immunostaining was also reduced at this time (Figure 3X

Table 2. Reduced gonadotrope and thyrotrope gene expression in newborn *Isl1*^{Prop1KO} pituitary glands

Gonadotrope lineage		Thyrotrope lineage		Other lineages	
Gene	Fold change	Gene	Fold change	Gene	Fold change
Gnrhr	0.12	*Cga*	0.20	*Ghrhr*	0.99
Lhb	0.14	*Rgs4*	0.52	*Gh*	0.99
Cga	0.20	*Tshr*	0.60	*Pomc*	0.99
Fshb	0.20	*Dio2*	0.63	*Tbx19*	0.97
Nr5a1	0.40	*Tshb*	0.66	*Prop1*	0.99
Foxl2	0.54			*Pou1f1*	0.92

and Supplemental Figure 3, R and S). The transient nature of the growth insufficiency could be due to regulation by hypothalamic-pituitary-thyroid axis feedback loops. At 7 weeks, the gonad and thyroid gland morphology appeared indistinguishable in mutants and controls, and the mice were fertile (Supplemental Figure 3, T–Y). In addition, despite abnormalities in intermediate lobe morphology, immunostaining for PAX7, MSH, SOX2, and SOX9 was normal in *Isl1*^{Prop1KO} mutants at E16.5 (Supplemental Figure 4).

Alternate cell fate underlies Isl1^{Prop1KO} *Rathke's cleft-like cyst formation*. The normal coexpression of ISL1 with the stem cell markers SOX2 and PROP1 in postnatal pituitary development suggests that the cysts in *Isl1*^{Prop1KO} pituitaries arise from progenitors. We analyzed expression of SOX2, SOX9, and PROP1 in *Isl1*^{Prop1KO} mice from initial cyst identification (P0), to early cyst formation (P7), through cyst maturation (7 weeks) (Figure 4, A–D, Supplemental Figure 5, A–H, and Supplemental Table 1). At birth, some of the small cysts evident in all *Isl1*^{Prop1KO} mutants were lined with cells positive for SOX2 and SOX9, and all were negative for PROP1. By P7, the cells lining the walls of the cyst were negative for SOX2 and PROP1, and only a subset of the cells expressed SOX9. Expression of FOXJ1 was identified in a few cells lining the cyst walls at P2, and it was more prominently expressed by P3 (Figure 4, E–H). As the cysts matured, some of the cells became positive for SOX2 or SOX9 (Supplemental Figure 5, I–L). These data support the idea that the cysts initially arise from the pituitary progenitor pool and that *Foxj1* is an early marker of altered cell fate.

We used the newborn pituitary RNA-Seq data set to discover changes in transcription that were associated with early cyst formation. Gene ontology (GO) analysis revealed that many of the genes with elevated expression in *Isl1*^{Prop1KO} pituitaries are involved in epithelial cell differentiation, proliferation, and development (Table 3 and Supplemental Table 2). The transcription factor genes in these enriched GO categories include *Mcidas*, *Foxa1*, *Trp63*, *Ehf*, *Foxj1*, *Elf5*, *Runx1*, *Nupr1*, *Dlx5*, *Ovol2*, and *Grhl1* (Table 4). *Mcidas*, or multicilin, drives the development of multiciliated cells, and it acts upstream of *Foxj1* (69). Many of these genes did not have detectable transcripts in the control data set (12/34 genes), suggesting that *Isl1* deficiency has permitted ectopic expression in the pituitary gland. For example, the bHLH transcription factor ASCL3 is not normally expressed in the pituitary gland, and it is highly specific for salivary gland tissue (The Human Protein Atlas, https://www.proteinatlas.org/ENSG00000176009-ASCL3/tissue). A complete list of differentially expressed transcripts is available in Supplemental Table 3

FOXA1 is a "pioneer" transcription factor that opens chromatin and is associated with development of endodermal tissues, such as lung and liver (reviewed in ref. 70). *Foxa1* transcripts were elevated 13.1-fold in newborn *Isl1*^{Prop1KO} pituitaries. Although FOXA1 has been proposed to repress expression of the GH-related chorionic somatomammotropin genes in the human pituitary gland (71), no *Foxa1* cDNA was detected in libraries prepared from normal E12.5 and E14.5 mouse pituitary glands and no *Foxa1* transcripts were detected in the pituitary gland at E11.5, E13.5, or E15.5 by in situ hybridization (ref. 72 and Allen Brain Atlas). We used immunostaining to examine *Foxa1* expression at E11.5 (Figure 4, I–N). We detected robust FOXA1 expression in the oral ectoderm and in only a few cells of Rathke's pouch. The FOXA1-positive cells in Rathke's pouch were located ventrally, at the point where the pouch and oral ectoderm separate, and they coexpressed ISL1. FOXA1 expression was unchanged in the *Isl1*^{Prop1KO} mice. Sonic hedgehog (SHH) is necessary for the induction of pituitary cell fate (73). It is expressed in the developing hypothalamus and oral ectoderm, but it is excluded from Rathke's pouch. No differences in SHH expression were detected between control and *Isl1*^{Prop1KO} (Figure 4, O and P).

Little is known about the expression or role of *Gata3* in pituitary development. *Gata3* is expressed in the αTSH pituitary thyrotrope cell line, and its expression is elevated in pituitary-specific *Gata2*-knockout mice in response to thyroid (65, 74). These observations, and the fact that GATA3 interacts with ISL1 to promote normal pyloric development (35), prompted us to examine *Gata3* expression in normal and *Isl1*^{PropKO} pituitaries. We detected GATA3 in the nuclei of cells at the ventral aspect of Rathke's pouch at E11.5, in the same region where ISL1 is expressed, but GATA3 expression was unchanged in the *Isl1*^{PropKO} mice (Figure 4, Q and R). However, the cells in the ventral aspect of Rathke's pouch of *Isl1*^{Prop1KO} mutants exhibited reduced expression of the cell cycle inhibitor CDKN1A (Figure 4, S and T). Thus, the spatial and temporal expression of GATA3 and ISL1 suggest that they could interact early in pituitary development, but the effect of *Isl1* deficiency on cell cycle exit is not attributable to changes in *Gata3* expression at that time.

We detected abnormal FOXA1 expression in *Isl1*^{Prop1KO} mutant pituitaries from E16.5 to 1 year (Figure 4, U–AB). No expression was detected at these times in normal pituitary glands. At E16.5, small clusters of FOXA1-positive cells were detected in *Isl1*^{Prop1KO} mutant pituitaries. FOXA1 expression was increased in the *Isl1*^{Prop1KO} mutants at E18.5, and it was clear that the FOXA1-positive cells were forming cysts. Thus, abnormal FOXA1 expression precedes expression of FOXJ1 by almost 1 week. FOXA1 expression was evident in cells lining the cysts at P3 and 7 weeks. FOXA1 and FOXJ1 were expressed in cells of mature cysts (Figure 4AB). We detected coexpression of FOXA1 and FOXJ1 in some cells as well as cells expressing only one of the factors.

We detected GATA3 expression at E18.5 and P0 in normal pituitary glands, but the immunoreactivity was predominately cytoplasmic, in contrast to the nuclear localization at E11.5 (Figure 4, AC–AF). Interestingly, we observed clusters of cells with both nuclear localized and cytoplasmic GATA3 in *Isl1*^{Prop1KO} mutants at E18.5 and P0. There was no visible nuclear GATA3 staining in the cells lining the cysts after P7, but cytoplasmic GATA3 expression was detectable after birth and in adult pituitary glands (Supplemental Figure 5,

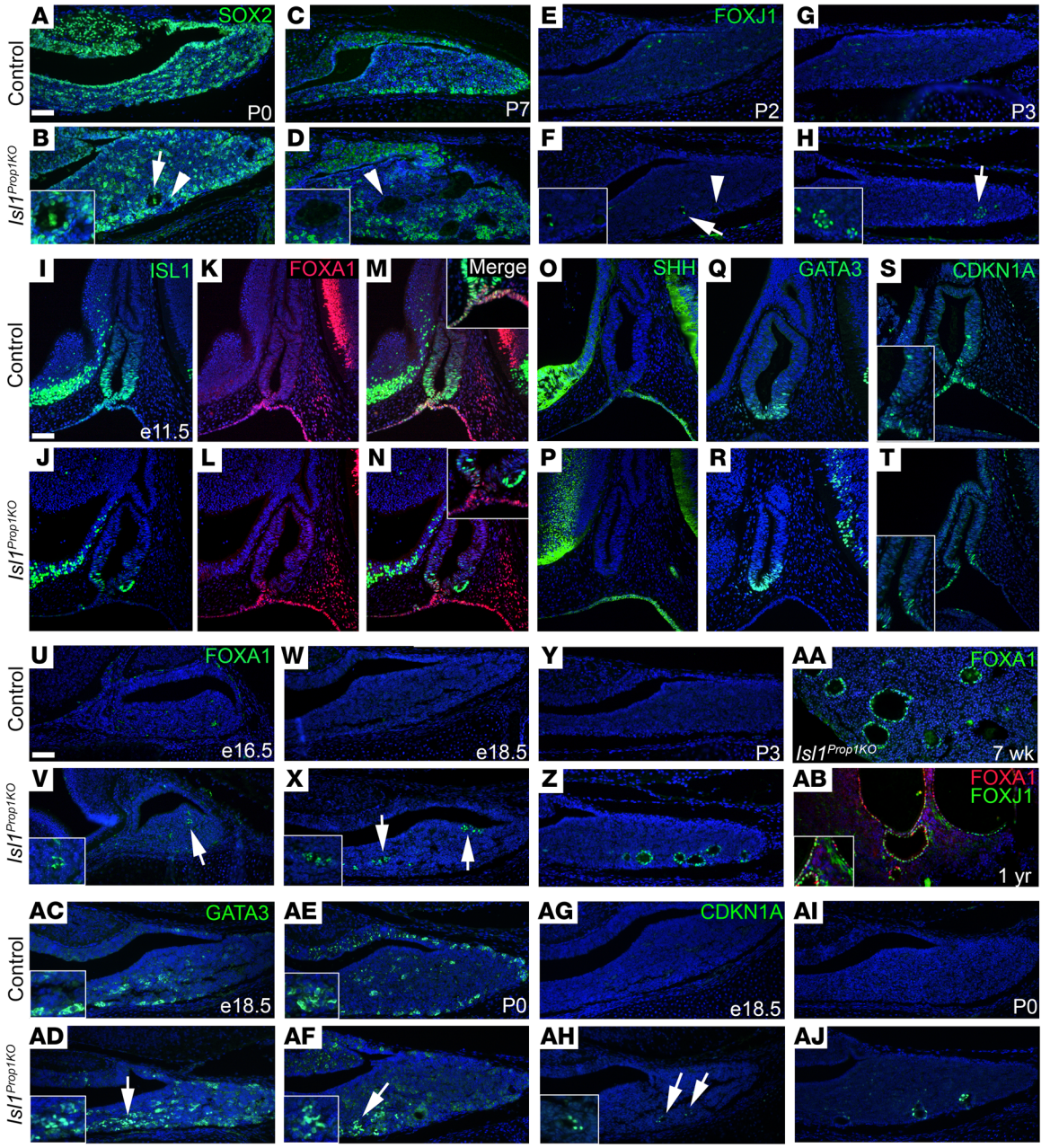

Figure 4. FOXA1 is the earliest marker of cyst development. (**A**–**D**) SOX2-positive cells are within the anterior lobe in control and *Isl1*^{Prop1KO} mutants. SOX2 is detected in some cysts walls at birth (**B**, $n = 5$), but not P7 (**D**, $n = 6$). (**E**–**H**) Minimal FOXJ1 immunostaining was detected in controls ($n = 3$) and increased in *Isl1*^{Prop1KO} cyst walls with age ($n = 3$). (**I** and **J**) ISL1$^+$ cells are in the ventral Rathke's pouch, oral ectoderm, and ventral diencephalon in E11.5 controls ($n = 6$), but few ISL1$^+$ cells are detected in the *Isl1*^{Prop1KO} mutant ($n = 6$). Similar E11.5 ISL1 immunostaining samples are described above. (**K**–**N**) FOXA1$^+$ cells are in the oral ectoderm, and a few ISL1$^+$FOXA1$^+$ cells are at the pouch/oral ectoderm separation in E11.5 controls ($n = 3$), but not in *Isl1*^{Prop1KO} ($n = 5$). (**O** and **P**) SHH expression in the oral ectoderm of E11.5 controls ($n = 8$) and *Isl1*^{Prop1KO} ($n = 9$). (**Q** and **R**) GATA3$^+$ ventral expression in E11.5 controls ($n = 3$) and *Isl1*^{Prop1KO} ($n = 3$). (**S** and **T**) CDKN1A$^+$ expression in E11.5 controls ($n = 3$) and *Isl1*^{Prop1KO} ($n = 6$). (**U**–**AA**) FOXA1 immunostaining was negative in controls (**U**, $n = 3$; **W**, $n = 4$; **Y**, $n = 3$). FOXA1$^+$ cells line cyst walls in *Isl1*^{Prop1KO} (**V**, $n = 4$; **X**, $n = 6$; **Z**, $n = 3$; **AA**, $n = 6$). (**AB**) FOXA1 and FOXJ1 stain in cyst walls at 1 year ($n = 5$). (**AC**–**AF**) Cytoplasmic GATA3 immunoreactivity is detected in E18.5 ($n = 6$) and P0 ($n = 6$) controls ($n = 6$), and nuclear staining is present in *Isl1*^{Prop1KO} ($n = 6$). (**AG**–**AJ**) CDNK1A immunostaining was not detected in E18.5 and P0 controls ($n = 3$, $n = 3$), but CDNK1A$^+$ cells were detected in *Isl1*^{Prop1KO} (inset, $n = 6$, $n = 3$). Scale bars: 50 μm (**A**–**H**, **I**–**T**, and **U**–**AJ**). Original magnification, ×400 (insets). Sagittal orientation (E11.5, E16.5), coronal orientation (E18.5-after birth). Arrows, immune-positive cells; arrowheads, immune-negative.

M–P). This suggests that ISL1 deficiency permits prolonged GATA3 localization in the nucleus during initial cyst development.

ISL1 and GATA3 bind to the same region of the *Cdkn1a* promoter in neuroblastoma cells and regulate its expression (75). Therefore, we analyzed expression of CDKN1A in the developing cysts. There was no detectable expression of CDKN1A in the control mice from E18.5 through 7 weeks. We discovered transient expression of CDKN1A in the cells forming cysts at E18.5

Table 3. GO enrichment: regulation of epithelial cell differentiation and development

Symbol	Gene name	Fold change	1	2	3	4	5
Krt15	Keratin 15	37.4×	x				
Krt5	Keratin 5	31.4×	x				
Mcidas	Multiciliate differentiation and DNA synthesis–associated cell cycle protein	19.9×	x				
Foxa1	Forkhead box A1	13.1×	x		x		
Krt4	Keratin 4	7.0×	x	x			
Ccno	Cyclin O	5.6×	x				
Agr2	Anterior Gradient 2	5.2×	x				
Krt23	Keratin 23	4.2×	x				
Trp63	Transformation-related protein 63	4.1×	x	x	x	x	x
Krt19	Keratin 19	3.9×	x				
Anxa1	Annexin A1	3.8×	x				
Upk1b	Uroplakin 1B	3.8×	x				
Ehf	Ets homologous factor	3.0×	x	x			
Lgals3	Lectin, galactose binding, soluble 3	3.0×	x				
Ccdc78	Coiled-coil domain containing 78	3.1×	x				
Foxj1	Forkhead box J1	2.5×	x		x	x	
Wnt7b	Wingless-type MMTV integration site family, member 7B	2.4×	x		x		
Elf5	E74-like factor 5	2.4×	x				
Dhrs9	Dehydrogenase/reductase (SDR family) member 9	2.4×	x				
Sfn	Stratifin	2.3×	x	x	x	x	
Runx1	Runt-related transcription factor 1	2.2×	x			x	
Dsp	Desmoplakin	2.1×	x				
Scel	Sciellin	2.1×	x				
Maff	V-Maf musculoaponeurotic fibrosarcoma oncogene family, protein F (avian)	2.0×	x			x	
Aqp3	Aquaporin 3	2.0×	x			x	
Spdef	SAM pointed domain–containing Ets transcription factor	1.9×	x		x		
Pkp1	Plakophilin 1	1.9×	x				
Tfcp2l1	Transcription factor CP2-like 1	1.8×	x		x		
Dsc3	Desmocollin 3	1.8×	x				
Krt17	Keratin 17	1.8×	x				
Krt8	Keratin 8	1.7×	x				
Ovol2	Ovo-like 2 (Drosophila)	1.6×	x	x		x	
Krt7	Keratin 7	1.6×	x				
Tgm1	Transglutaminase 1, K polypeptide	1.6×	x	x			x
Tst	Thiosulfate sulfurtransferase, mitochondrial	1.6×	x				
Ceacam1	Carcinoembryonic antigen-related cell adhesion molecule 1	1.5×	x	x		x	
Grhl1	Grainyhead-like 1 (Drosophila)	1.5×	x			x	
Upk3a	Uroplakin 3A	1.5×	x				
Fgfbp1	Fibroblast growth factor–binding protein 1	2.8×		x			
Dlx5	Distal-less homeobox 5	1.8×		x			x
Plxnb3	Plexin B3	1.8×		x			x
F3	Coagulation factor III	1.5×		x			x
Serpinb1b	Serine (or cysteine) peptidase inhibitor, clade B, member 1b	7.0×		x			
Tacstd2	Tumor-associated calcium signal transducer 2	4.0×		x			
Nupr1	Nuclear protein transcription regulator 1	2.2×		x			

1, Epithelial cell differentiation; 2, epithelial cell proliferation; 3, epithelial cell development; 4, regulation of epithelial cell differentiation; 5, positive regulation of epithelial cell proliferation.

and P0, but no expression at P7 or 7 weeks (Figure 4, AG–AJ, and Supplemental Figure 4, Q–T). Thus, FOXA1 is the earliest marker of cyst formation, and both GATA3 and CDKN1A are transiently expressed during initial cyst formation.

hRCCs express FOXA1. Twenty-two patients were diagnosed with hRCC at Kagoshima University. Samples of resected tissue from each patient were analyzed for markers characteristic of hRCC to ensure that the available sections contained cystic regions appropriate for further analysis. Sixteen out of the 22 samples of resected material contained regions positive for expression of the classical hRCC markers: acetylated tubulin, cytokeratin 8, or FOXJ1. The cysts were lined with ciliated, cuboidal, or columnar epithelium. They were positive for cytokeratin 8, and the cilia were marked with acetylated tubulin. These samples were select-

Table 4. Transcription factors elevated in *Isl1*^{Prop1KO}

Gene name	Fold change	Ectopic
Multiciliate differentiation and DNA synthesis–associated cell cycle protein (*Mcidas*)[A,B]	19.9×	Yes
Forkhead box A1 (*Foxa1*)[A,B]	13.1×	Yes
Achaete-scute complex homolog 3 (*Ascl3*)[A]	11.9×	Yes
Lactotransferrin (*Ltf*)[A]	9.1×	Yes
Forkhead box I1 (*Foxi1*)[A]	7.8×	Yes
Protein phosphatase 1, regulatory (inhibitor) subunit 1B (*Ppp1r1b*)[A]	4.2×	Yes
Transformation related protein 63 (*Trp63*)[A,B]	4.1×	Yes
Forkhead box G1 (*Foxg1*)[A]	3.7×	Yes
Ets homologous factor (*Ehf*)[B]	3.0×	No
Forkhead box J1 (*Foxj1*)[B]	2.5×	No
Trans-acting transcription factor 8 (*Sp8*)[A]	2.4×	Yes
E74-like factor 5 (*Elf5*)[A,B]	2.4×	Yes
Mitogen-activated protein kinase 15 (*Mapk15*)	2.4×	No
Runt-related transcription factor 1 (*Runx1*)[B]	2.2×	No
Nuclear protein transcription regulator 1 (*Nupr1*)[B]	2.2×	No
Myeloid leukemia factor 1 (*Mlf1*)	2.0×	No
Sperm-associated antigen 8 (*Spag8*)	1.9×	No
Nuclear factor, erythroid derived 2, like 3 (*Nfe2l3*)	1.9×	No
Distal-less homeobox 5 (*Dlx5*)[B]	1.8×	No
Transcription factor CP2-like 1 (*Tfcp2l1*)	1.8×	No
Myeloblastosis oncogene (*Myb*)	1.7×	No
PDZ and LIM domain 1 (elfin) (*Pdlim1*)	1.7×	No
Jun B proto-oncogene (*Junb*)	1.7×	No
Pirin (*Pir*)	1.7×	No
A disintegrin and metallopeptidase domain 8 (*Adam8*)	1.6×	No
Doublesex and Mab-3 related transcription factor 2 (*Dmrt2*)[A]	1.6×	Yes
Ovo-like 2 (*Ovol2*)[B]	1.6×	No
Parathyroid hormone-like peptide (*Pthlh*)	1.6×	No
Orthodenticle homolog 1 (*Otx1*)[A]	1.5×	Yes
Grainyhead-like 1 (*Grhl1*)[B]	1.5×	No
Zinc finger and BTB domain–containing 16 (*Zbtb16*)	1.5×	No
Tumor necrosis factor, alpha-induced protein 3 (*Tnfaip3*)	1.5×	No

[A]Transcripts normally not present in the pituitary. [B]Transcription factors elevated in GO term associated with ciliated epithelium. Genes are listed according to fold change, beginning with the gene having the highest change in expression.

ed for further analysis of SOX2, SOX9, FOXA1, GATA3, and CDKN1A expression (Table 5). Fifteen of the 16 cases analyzed (94%) showed striking similarity to the *Isl1*^{Prop1KO} mutants, including expression of FOXA1 (Figure 5, A–R, and Supplemental Figure 6, A–R). Many of the cells were positive for both SOX2 and SOX9, and most of the cells were positive for either FOXA1, FOXJ1, or both. In addition, many cells within the cysts were positive for CDKN1A, and only a few were also positive for GATA3, as was predicted based on the transient expression in the *Isl1*^{Prop1KO} mutants. One of the 16 samples was positive for CDKN1A, but negative for the remaining markers.

To determine whether FOXA1 and GATA3 expression are unique to hRCCs, we analyzed expression in human craniopharyngioma samples of both the ACP (7 samples) and PCP subtypes (5 samples) (Figure 5, S–X, and Supplemental Figure 6, S–X). Craniopharyngioma samples serve as a suitable control because, in the clinical setting, it can be difficult to discriminate between RCC and craniopharyngiomas (76), making identification of distinguishing markers relevant to proper diagnosis. CDKN1A expression has been detected in craniopharyngiomas (57, 77, 78), and immunostaining for CDKN1A provides a quality control for the integrity of the tumor samples. The number of samples used was based on availability. Eleven of the 12 craniopharyngiomas analyzed were positive for CDKN1A staining. These 11 samples were negative for both FOXA1 and GATA3, suggesting expression of these markers is unique to hRCCs. In addition, *FOXA1* expression was not detected in RNA-Seq data sets from human ACP samples versus controls and a mouse model of ACP versus control mouse pituitary, confirming its specificity to RCC (57). Similarities between *Isl1*^{Prop1KO} RCC-like and hRCC support the role of ISL1 in the formation of RCCs and provide markers for identification in patients with suspected RCC formation.

Discussion

LIM homeodomain transcription factors play an important role in the development and cell specification of the pituitary gland and many other organ systems. *Lhx3* and *Lhx4* are essential for cell proliferation and cell specification in Rathke's pouch, and *Lhx2* is required for formation of the infundibulum and posterior lobe of the pituitary gland (22, 24, 27, 40). ISL1 is expressed in both Rathke's pouch and the adjacent ventral diencephalon. Here, we show, using 3 different mouse models, that, although Rathke's pouch forms in the absence of *Isl1*, ISL1 has multiple, critical roles in pituitary gland development (Figure 6). It is important for Rathke's pouch morphology, specification of the thyrotrope and gonadotrope cell fates, and suppression of alternate, nonpituitary cell fates. *Isl1* deficiency drives the development of Rathke's cleft-like cysts with 100% penetrance.

Both *Prop1-cre*– and *Hesx1-cre*–mediated deletion of *Isl1* cause obvious dysmorphology and modest reduction in growth of Rathke's pouch. *Isl1* deficiency causes abnormal expression of *Ccnd1*, reduced cell proliferation, and increased apoptosis. The approximately 22% reduction in pouch size of pituitary-specific *Isl1* deletion contrasts with the severe Rathke's pouch hypoplasia reported for the global *Isl1*$^{-/-}$ mutant embryos. However, poor pouch formation in *Isl1*$^{-/-}$ embryos could be secondary to poor overall embryonic growth, heart failure, early death, and/or ventral diencephalon defects (38, 41). The basis for the pituitary dysmorphology in pituitary-specific models of *Isl1* deficiency is unknown, but it appears that some progenitor cells lose the typical flattened, epithelial-like shape and adopt rounded shapes organized in clusters. ISL1 has a role in growth of the pituitary and

Table 5. Summary of hRCC characterization

Age	Sex	Acetylated tubulin	Cytokeratin 8	FOXA1	FOXJ1	SOX2	SOX9	GATA3	CDKN1A
53	M	++	++	–	–	–	–	–	+
32[A]	M	++	++	–	–	++	++	–	–
		++	++	++	+	++	++	–	++
		+	++	+	+	+	+	–	+
57	M	++	++	++	++	++	++	–	+
60	M	++	++	++	++	++	++	–	++
77	F	++	++	++	++	++	++	–	++
59	F	++	++	++	++	++	++	–	+
27	M	++	++	+	++	++	++	–	++
63	F	++	++	++	++	++	++	–	++
30	F	++	++	++	++	++	++	–	++
58	M	++	++	++	++	++	++	–	+
18	F	++	++	++	++	+	+	++	+
23	F	+	++	++	++	++	++	–	+
37	F	++	++	++	++	++	++	++	+
61	F	++	++	++	++	+	+	++	++

[A]RCC recurred twice; a sample was obtained from each procedure.

other organs, including the nervous system, uteric bud, pancreas, and heart (31, 38, 79–82).

The specification of the thyrotrope and gonadotrope lineages was markedly reduced by both *Prop1-cre*–mediated and tamoxifen-induced deletion of *Isl1*. The characteristic hormones CGA, TSH, and LH were reduced as well as the early lineage-specific transcription factors NR5A1 and FOXL2. The reduced expression of *Nr5a1* and *Foxl2* was sufficient to explain the failure of gonadotrope differentiation because *Nr5a1* deficiency results in failure to express LH and FSH and gonadotrope-specific *Foxl2* deficiency causes subfertility with marked reduction in FSH (83–85). Direct regulation of *Nr5a1* or *Foxl2* expression by ISL1 has not been explored, but ISL1 does interact with LHX3 and NR5A1 to activate expression of a key gonadotrope marker: *Gnrhr* (86). GATA2 is important for gonadotrope and thyrotrope specification (2, 64, 65), but we did not detect an effect of *Isl1* deficiency on *Gata2* expression. It is possible that ISL1 drives thyrotrope fate directly.

We present a developmental model of Rathke's cleft-like cysts. Both *Prop1-cre*– and *Hesx1-cre*–mediated deletion of *Isl1* in the pituitary gland were associated with the appearance of multiple cyst-like structures in late gestation and early postnatal life of 100% of the mutants. The cells lining the cysts expressed typical markers of RCC, including cytokeratins, acetylated tubulin, and FOXJ1. Mucinous and ciliated cells were both present, and the sizes of the cysts increased with age. The RCC-like structures appeared to derive from pituitary progenitors that express SOX2 and SOX9. The expression of these progenitor markers was transient in the cysts, disappearing postnatally and then reappearing in cells lining the cysts as the animals approached adulthood. Thus, ISL1 is necessary to suppress alternate cell fates in pituitary progenitors. ISL1 represses alternate cell fates in neuronal and tooth development, although the mechanism in those tissues is unknown (87, 88).

FOXA1 is the earliest marker of mouse Rathke's cleft-like cyst formation. The aberrant expression of FOXA1 was followed by abnormal nuclear localization of GATA3, abnormal activation of CDKN1A expression, and finally ectopic FOXJ1 expression. We hypothesize that *Isl1* normally suppresses expression of *Foxa1* in the pituitary primordium and that *Foxa1* expression is sufficient to drive alternate cell fate, in part by activation of FOXJ1 expression. Rathke's cleft-like cysts are similar in appearance to the ciliated epithelium from lung or salivary gland, and FOXA1, together with FOXA2, activates FOXJ1 expression in developing lung, which is necessary to drive differentiation of the respiratory epithelium (89–93). Moreover, ectopic expression of SOX2 drives FOXJ1 expression in lung development (94), and modulation of SOX9 expression during lung development is necessary to balance proliferation and differentiation (95, 96). Taken together, these observations support our hypothesis that FOXA1 is a driver of alternate cell fate in the pituitary gland.

Gata2 and *Gata3* are paralogs, and they have overlapping roles in the development of neurons of the inner ear and trophoblast progenitors (97, 98). The role of GATA3 in pituitary development is unknown, but ISL1 and GATA3 interact to drive development in some other tissues (35, 75). We speculate that (a) ISL1 normally interacts with GATA2 and GATA3 to drive pituitary cell specification, and (b) ISL1 deficiency may permit GATA3 to participate in driving mucinous and ciliated epithelial cell fate. Normally, the subcellular localization of GATA3 shifts from the nucleus to the cytoplasm after pituitary cells commit to thyrotrope and gonadotrope fates. The abnormal persistence of GATA3 in the nucleus of pituitary progenitors may permit interaction with FOXA1 to drive alternate fate, as GATA3 expression is essential for luminal cell fate in mammary epithelium (99). Pituitary-specific knockouts of *Gata3* will be necessary to clarify its role in pituitary development.

hRCC are commonly discovered after the cyst is fully formed and symptomatic, making it impossible to study the development of cysts in patients. The $Isl1^{Prop1KO}$ mice provided an excellent opportunity for studying Rathke's cleft-like cyst development and

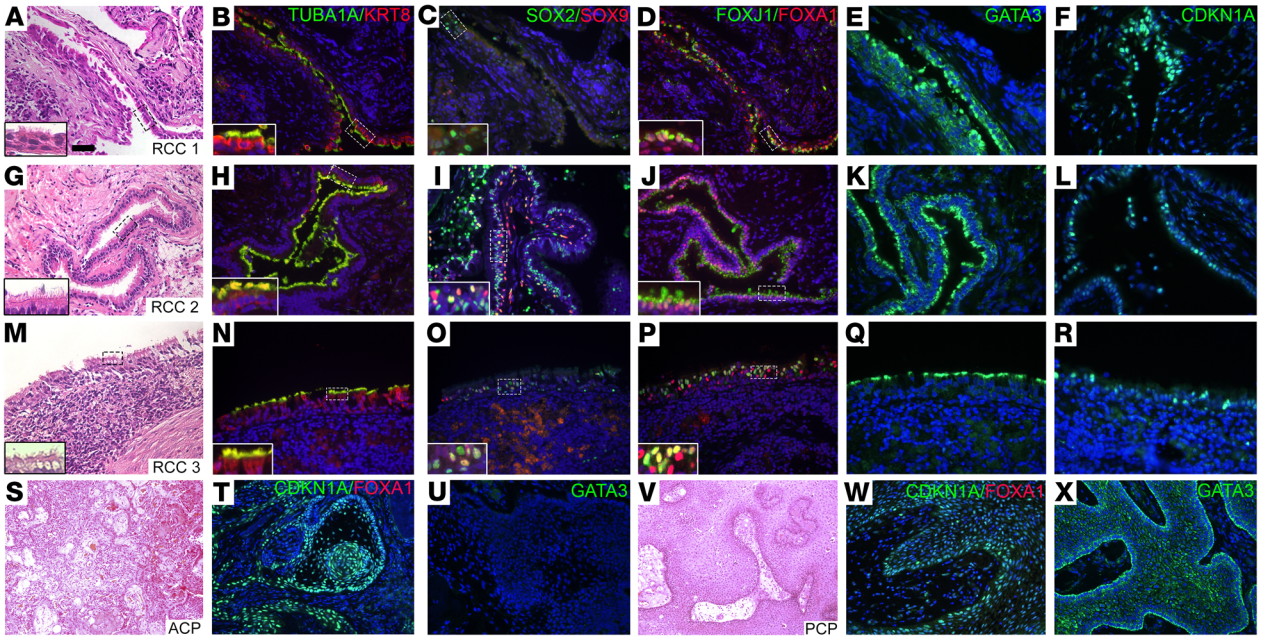

Figure 5. hRCCs express FOXA1. (**A**–**R**) Classification of hRCC samples (n = 16) was confirmed by staining with H&E to detect ciliated cells (insets) (**A**, **G**, and **M**) and costaining with antibodies for cytokeratin8 and acetylated tubulin (**B**, **H**, and **N**). Costaining with antibodies for progenitor markers SOX2 and SOX9 detected many positive cells (**C**, **I**, and **O**). Costaining with antibodies FOXJ1 and FOXA1 detected positive cells lining the cysts (**D**, **J**, and **P**). Immunostaining for GATA3 (**E**, **K**, and **Q**) and CDKN1A (**F**, **L**, and **R**) detected positive cells lining the cysts in some, but not all samples. (**S**–**X**) Surgical samples from craniopharyngiomas of both the ACP (n = 7) (**S**–**U**) and PCP (n = 5) (**V**–**X**) subtypes were stained with H&E, costained for CDKN1A and FOXA1, and immunostained for GATA3. Samples were positive for CDKN1A and negative for both FOXA1 and GATA3. Scale bar: 50 μm.

identifying markers that can be used in the diagnosis of hRCC. We detected FOXA1 expression in hRCCs in 94% of the samples we had available for study, suggesting that FOXA1 may have a role in driving cyst development in humans. We did not detect FOXA1 in craniopharyngiomas, and *FOXA1* transcripts were not reported in craniopharyngioma data sets, indicating that this marker is specific for RCCs (57). In contrast, FOXJ1 is not specific to hRCC. It has been identified in rare PCP craniopharyngiomas, and transcripts were enriched in the human ACP versus control pituitary RNA-Seq data set (57, 60). Sporadic expression of GATA3, CDKN1A, SOX2, and SOX9 in hRCCs is consistent with the transient and/or developmental changes in expression of these markers in the *Isl1*^{Prop1KO} mutant model. Thus, the similarities between *Isl1*^{Prop1KO} mutant and hRCCs has provided insight into cyst formation and identified additional diagnostic markers to be used in pathological characterization.

Patients with RCCs have a single cyst, whereas the *Isl1*-deficient mice had multiple cysts. hRCCs are usually asymptomatic, and if hormone deficiency occurs, it is attributable to organ compression by the cyst. This contrasts with the gonadotropin and thyrotropin deficiencies in mice with pituitary-specific deletion of *Isl1*, which are caused by the failure of *Isl1* to drive those pituitary cell fates. These differences may be attributable to differences in the underlying etiology. In humans, somatic mutation in rare progenitors may cause loss of a transcription factor and/or permissive activation of FOXA1 to drive ciliated and mucinous cell fates. In contrast, we deleted both alleles of *Isl1* early in pituitary development, which could permit multiple progenitors to switch fate at the same time that differentiation to gonadotropes and thyrotropes fails. The number of cells that exhibit altered transcription factor expression could be a key variable in whether the mutant cells undergo apoptosis or survive and differentiate into alternate cell fates. For example, in *Drosophila*, neighboring cells detect ectopic transcription factor expression (100). If the number of cells with ectopic transcription factor expression is small, the abnormal cells are induced to undergo apoptosis. If misexpression of transcription factor(s) is more widespread, the surrounding, normal cells induce abscission of the abnormal cells, and cysts form. Similar mechanisms may underlie the enhanced apoptosis and cyst formation in *Isl1*^{Prop1KO} pituitary glands. During development, we observed elevated apoptosis of *Isl1*-deficient cells, while around birth, cells abnormally expressing FOXA1 appeared to be encapsulated into cysts.

In sum, we have established the role of *Isl1* in multiple steps in pituitary development: Rathke's pouch morphology and growth, induction of lineage-specific transcription factors for gonadotrope and thyrotrope specification, and suppression of abnormal ciliated and mucinous cell fates. This developmental model of Rathke's cleft-like cyst formation accurately predicted FOXA1 as a marker of this common abnormality in human pituitary glands.

Methods

Additional methods can be found in Supplemental Methods.

RNA-Seq. RNA-Seq data have been deposited in the NCBI's Gene Expression Omnibus (GEO GSE149019; ref. 101).

Study approval. All mouse studies were approved by the University of Michigan IACUC (PRO00008714) or by the Facultad de Ciencias Exactas y Naturales–University of Buenos Aires Comisión

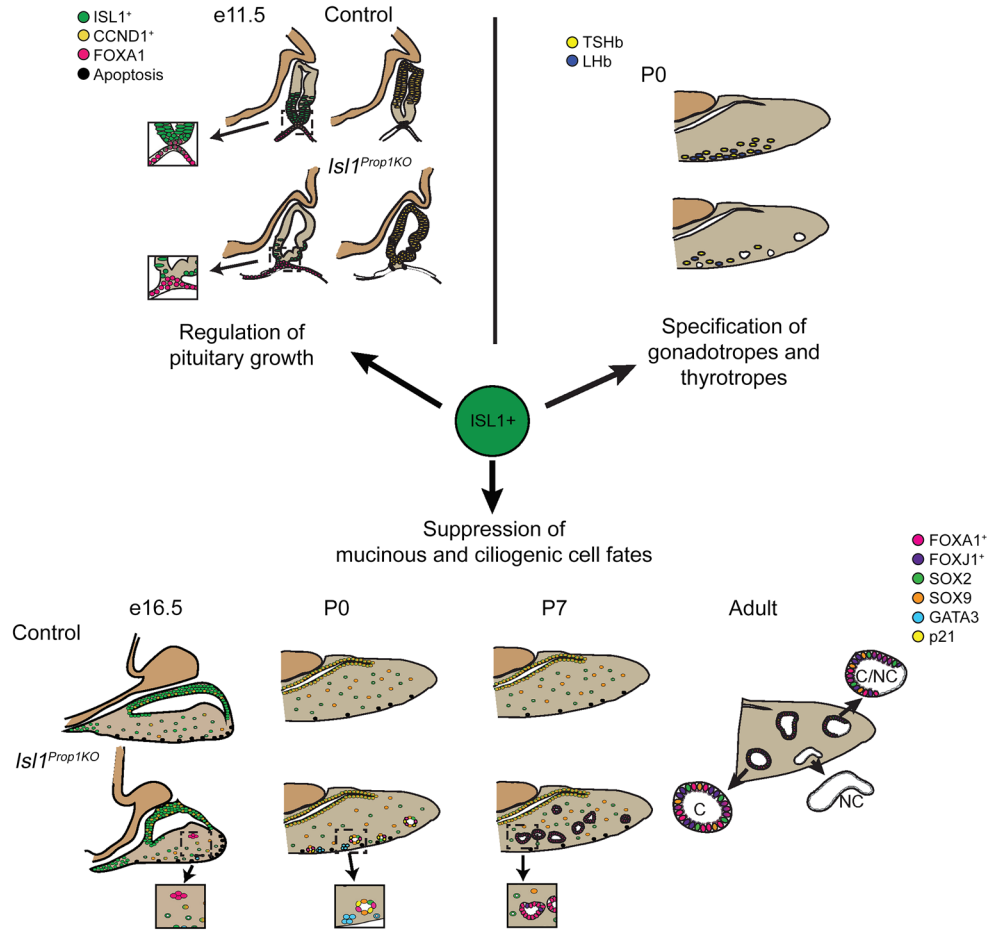

Figure 6. ISL1 regulates multiple aspects of pituitary gland development. ISL1 regulates growth of Rathke's pouch. ISL1 expression is initially activated throughout the pouch (E10.5) (41). By E11.5, ISL1 expression is restricted to the ventral aspect of Rathke's pouch (green), where cells begin to differentiate and express CGA. This ISL1 domain is juxtaposed ventrally by FOXA1 expression in the nearby oral ectoderm and dorsally by cyclin D1 (CCND1, yellow) expression in proliferating progenitor cells transitioning from the G_1 to the S phase. In the absence of ISL1 expression, the domain of cyclin D1 expression is expanded and there are ectopic sites of apoptosis (black). ISL1 stimulates specification of gonadotrope and thyrotrope lineages by elevating expression of NR5A1 and FOXL2. ISL1-deficient pituitaries have reduced expression of NR5A1 and FOXL2, but no obvious change in GATA2 or GATA3 expression. The reduction in lineage-specific transcription factor gene expression is associated with differentiation of very few thyrotropes (yellow) and gonadotropes (blue) cells at birth. ISL1 suppresses SOX2-expressing progenitors from adopting alternate cell fates. Loss of ISL1 leads to abnormal expression of FOXA1 (red), atypical localization of GATA3 in the nucleus (blue), and activation of p21 expression (CDKN1A, yellow), which is associated with cell cycle exit (G_0). These cells maintain FOXA1 expression, activate FOXJ1, and execute a ciliogenic, mucinous cell fate, resulting in ciliated and nonciliated RCCs.

Institucional para el Cuidado y Uso de Animales de Laboratorio (Buenos Aires, Argentina) (protocol 68). Mice were housed in an AALAC-approved animal facility at the University of Michigan and at the Bioterio Central of Facultad de Ciencias Exactas y Naturales–University of Buenos Aires. Informed consent for collection of human pituitary specimens was approved by the ethical committee of Kagoshima University (reference 180135). Anonymized specimens were sent to the University of Michigan for immunostaining, which was classified as exempt by the IRB-MED.

Author contributions

MLB and SAC conceived the study. MLB analyzed the *Isl1*^{Prop1KO} mice and *Isl1*^{Hesx1creKO} mice. ACC and FSJDS analyzed the *CAG-ERT-2cre; Isl1*^{fx} mice. SF and KY contributed the hRCC and craniopharyngioma samples. MLB and HB analyzed the hRCC samples. MLB analyzed the craniopharyngioma samples. MLB and SAC wrote the original manuscript, and MLB, HB, SF, KY, ACC, FSJDS, and SAC reviewed and edited the manuscript.

Acknowledgments

We thank Robert Lyons and the University of Michigan Advanced Genomics Core and Rich McEachin from the Bioinformatics Core for their help in the planning and analysis of the RNA-Seq experiments. This work was supported by NIH R01 HD034283 (to SAC), the Japan Society for the Promotion of Science Overseas Research Fellowship (to HB), and National Agency for Scientific and Technological Promotion PICT 2013-2171 and CONICET (to FSJDS).

Address correspondence to: Sally A. Camper, University of Michigan, Department of Human Genetics, 5805 Medical Science II Building, 1241 Catherine Street, Ann Arbor, Michigan 48109-5618, USA. Phone: 734.764.4434; Email: scamper@umich.edu

1. Han SJ, Rolston JD, Jahangiri A, Aghi MK. Rathke's cleft cysts: review of natural history and surgical outcomes. *J Neurooncol*. 2014;117(2):197–203.
2. Kanter AS, Sansur CA, Jane JAJ, Laws ERJ. Rathke's cleft cysts. *Front Horm Res*. 2006;34:127–157.
3. Larkin S, Karavitaki N, Ansorge O. Rathke's cleft cyst. *Handb Clin Neurol*. 2014;124:255–269.
4. Trifanescu R, Ansorge O, Wass JA, Grossman AB, Karavitaki N. Rathke's cleft cysts. *Clin Endocrinol (Oxf)*. 2012;76(2):151–160.
5. Aho CJ, Liu C, Zelman V, Couldwell WT, Weiss MH. Surgical outcomes in 118 patients with Rathke cleft cysts. *J Neurosurg*. 2005;102(2):189–193.
6. Kim JE, et al. Surgical treatment of symptomatic Rathke cleft cysts: clinical features and results with special attention to recurrence. *J Neurosurg*. 2004;100(1):33–40.
7. Manjila S, et al. Intratumoral Rathke's cleft cyst remnants within craniopharyngioma, pituitary adenoma, suprasellar dermoid, and epidermoid cysts: a ubiquitous signature of ectodermal lineage or a transitional entity? *Neurosurgery*. 2019;85(2):180–188.
8. Benveniste RJ, King WA, Walsh J, Lee JS, Naidich TP, Post KD. Surgery for Rathke cleft cysts: technical considerations and outcomes. *J Neurosurg*. 2004;101(4):577–584.
9. Harrison MJ, Morgello S, Post KD. Epithelial cystic lesions of the sellar and parasellar region: a continuum of ectodermal derivatives? *J Neurosurg*. 1994;80(6):1018–1025.
10. Osborn AG, Preece MT. Intracranial cysts: radiologic-pathologic correlation and imaging approach. *Radiology*. 2006;239(3):650–664.
11. Verlinsky Y, et al. Preimplantation diagnosis for sonic hedgehog mutation causing familial holoprosencephaly. *N Engl J Med*. 2003;348(15):1449–1454.
12. Vincent A, et al. OTX2 mutations cause autosomal dominant pattern dystrophy of the retinal pigment epithelium. *J Med Genet*. 2014;51(12):797–805.
13. Schaetti P, Argentino-Storino A, Heinrichs M, Mirea D, Popp A, Karbe E. Aberrant craniopharyngeal structures within the neurohypophysis of rats. *Exp Toxicol Pathol*. 1995;47(2–3):129–137.
14. Watanabe YG. The occurrence and developmental origin of epithelial cysts in the rat and mouse adenohypophysis. *Arch Histol Cytol*. 1991;54(5):511–518.
15. VanGilder JC, Inukai J. Growth characteristics of experimental intracerebrally transplanted oral epithelium. *J Neurosurg*. 1973;38(5):608–615.
16. Akita S, et al. Pituitary-directed leukemia inhibitory factor transgene forms Rathke's cleft cysts and impairs adult pituitary function. A model for human pituitary Rathke's cysts. *J Clin Invest*. 1997;99(10):2462–2469.
17. Yano H, Readhead C, Nakashima M, Ren SG, Melmed S. Pituitary-directed leukemia inhibitory factor transgene causes Cushing's syndrome: neuro-immune-endocrine modulation of pituitary development. *Mol Endocrinol*. 1998;12(11):1708–1720.
18. Nicola NA, Babon JJ. Leukemia inhibitory factor (LIF). *Cytokine Growth Factor Rev*. 2015;26(5):533–544.
19. Tran A, Kovacs K, Stefaneanu L, Kontogeorgos G, Scheithauer BW, Melmed S. Expression of leukemia inhibitory factor in craniopharyngioma. *Endocr Pathol*. 1999;10(2):103–108.
20. Lodge EJ, Russell JP, Patist AL, Francis-West P, Andoniadou CL. Expression analysis of the hippo cascade indicates a role in pituitary stem cell development. *Front Physiol*. 2016;7:114.
21. Lodge EJ, et al. Homeostatic and tumourigenic activity of SOX2+ pituitary stem cells is controlled by the LATS/YAP/TAZ cascade. *Elife*. 2019;8:e43996.
22. Ellsworth BS, Butts DL, Camper SA. Mechanisms underlying pituitary hypoplasia and failed cell specification in Lhx3-deficient mice. *Dev Biol*. 2008;313(1):118–129.
23. Li H, et al. Gsh-4 encodes a LIM-type homeodomain, is expressed in the developing central nervous system and is required for early postnatal survival. *EMBO J*. 1994;13(12):2876–2885.
24. Raetzman LT, Ward R, Camper SA. Lhx4 and Prop1 are required for cell survival and expansion of the pituitary primordia. *Development*. 2002;129(18):4229–4239.
25. Sheng HZ, et al. Multistep control of pituitary organogenesis. *Science*. 1997;278(5344):1809–1812.
26. Sheng HZ, et al. Specification of pituitary cell lineages by the LIM homeobox gene Lhx3. *Science*. 1996;272(5264):1004–1007.
27. Zhao Y, Mailloux CM, Hermesz E, Palkóvits M, Westphal H. A role of the LIM-homeobox gene Lhx2 in the regulation of pituitary development. *Dev Biol*. 2010;337(2):313–323.
28. Ahlgren U, Pfaff SL, Jessell TM, Edlund T, Edlund H. Independent requirement for ISL1 in formation of pancreatic mesenchyme and islet cells. *Nature*. 1997;385(6613):257–260.
29. Karlsson O, Thor S, Norberg T, Ohlsson H, Edlund T. Insulin gene enhancer binding protein Isl-1 is a member of a novel class of proteins containing both a homeo- and a Cys-His domain. *Nature*. 1990;344(6269):879–882.
30. Chumak T, et al. Deterioration of the medial olivocochlear efferent system accelerates age-related hearing loss in Pax2-Isl1 transgenic mice. *Mol Neurobiol*. 2016;53(4):2368–2383.
31. Du A, et al. Islet-1 is required for the maturation, proliferation, and survival of the endocrine pancreas. *Diabetes*. 2009;58(9):2059–2069.
32. Elshatory Y, Everhart D, Deng M, Xie X, Barlow RB, Gan L. Islet-1 controls the differentiation of retinal bipolar and cholinergic amacrine cells. *J Neurosci*. 2007;27(46):12707–12720.
33. Elshatory Y, Gan L. The LIM-homeobox gene Islet-1 is required for the development of restricted forebrain cholinergic neurons. *J Neurosci*. 2008;28(13):3291–3297.
34. Kawakami Y, et al. Islet1-mediated activation of the β-catenin pathway is necessary for hindlimb initiation in mice. *Development*. 2011;138(20):4465–4473.
35. Li Y, et al. LIM homeodomain transcription factor Isl1 directs normal pyloric development by targeting Gata3. *BMC Biol*. 2014;12:25.
36. Mitsiadis TA, Angeli I, James C, Lendahl U, Sharpe PT. Role of Islet1 in the patterning of murine dentition. *Development*. 2003;130(18):4451–4460.
37. Nasif S, et al. Islet 1 specifies the identity of hypothalamic melanocortin neurons and is critical for normal food intake and adiposity in adulthood. *Proc Natl Acad Sci USA*. 2015;112(15):E1861–E1870.
38. Pfaff SL, Mendelsohn M, Stewart CL, Edlund T, Jessell TM. Requirement for LIM homeobox gene Isl1 in motor neuron generation reveals a motor neuron-dependent step in interneuron differentiation. *Cell*. 1996;84(2):309–320.
39. Ericson J, Norlin S, Jessell TM, Edlund T. Integrated FGF and BMP signaling controls the progression of progenitor cell differentiation and the emergence of pattern in the embryonic anterior pituitary. *Development*. 1998;125(6):1005–1015.
40. Gergics P, Brinkmeier ML, Camper SA. Lhx4 deficiency: increased cyclin-dependent kinase inhibitor expression and pituitary hypoplasia. *Mol Endocrinol*. 2015;29(4):597–612.
41. Takuma N, et al. Formation of Rathke's pouch requires dual induction from the diencephalon. *Development*. 1998;125(23):4835–4840.
42. Castinetti F, et al. ISL1 is necessary for maximal thyrotrope response to hypothyroidism. *Mol Endocrinol*. 2015;29(10):1510–1521.
43. Gergics P, Christian HC, Choo MS, Ajmal A, Camper SA. Gene expression in mouse thyrotrope adenoma: transcription elongation factor stimulates proliferation. *Endocrinology*. 2016;157(9):3631–3646.
44. Andoniadou CL, et al. Sox2(+) stem/progenitor cells in the adult mouse pituitary support organ homeostasis and have tumor-inducing potential. *Cell Stem Cell*. 2013;13(4):433–445.
45. Fauquier T, Rizzoti K, Dattani M, Lovell-Badge R, Robinson IC. SOX2-expressing progenitor cells generate all of the major cell types in the adult mouse pituitary gland. *Proc Natl Acad Sci USA*. 2008;105(8):2907–2912.
46. Pérez Millán MI, Brinkmeier ML, Mortensen AH, Camper SA. PROP1 triggers epithelial-mesenchymal transition-like process in pituitary stem cells. *Elife*. 2016;5:e14470.
47. Rizzoti K, Akiyama H, Lovell-Badge R. Mobilized adult pituitary stem cells contribute to endocrine regeneration in response to physiological demand. *Cell Stem Cell*. 2013;13(4):419–432.
48. Davis SW, Keisler JL, Pérez-Millán MI, Schade V, Camper SA. All hormone-producing cell types of the pituitary intermediate and anterior lobes derive from Prop1-expressing progenitors. *Endocrinology*. 2016;157(4):1385–1396.
49. Pan L, Deng M, Xie X, Gan L. ISL1 and BRN3B co-regulate the differentiation of murine retinal ganglion cells. *Development*. 2008;135(11):1981–1990.
50. Andoniadou CL, et al. Lack of the murine homeobox gene Hesx1 leads to a posterior transformation of the anterior forebrain. *Development*. 2007;134(8):1499–1508.
51. Brzezinski JA, Prasov L, Glaser T. Math5 defines the ganglion cell competence state in a subpopulation of retinal progenitor cells exiting the cell cycle. *Dev Biol*. 2012;365(2):395–413.
52. Prasov L, Glaser T. Pushing the envelope of retinal ganglion cell genesis: context dependent function of Math5 (Atoh7). *Dev Biol*. 2012;368(2):214–230.

53. Mukherjee JJ, et al. Clinical, radiological and pathological features of patients with Rathke's cleft cysts: tumors that may recur. *J Clin Endocrinol Metab*. 1997;82(7):2357–2362.
54. Shin JL, Asa SL, Woodhouse LJ, Smyth HS, Ezzat S. Cystic lesions of the pituitary: clinicopathological features distinguishing craniopharyngioma, Rathke's cleft cyst, and arachnoid cyst. *J Clin Endocrinol Metab*. 1999;84(11):3972–3982.
55. Uematsu Y, Komai N, Hirano A, Corona-Rojas RR, Llena JF. [Epithelial cyst in the central nervous system--characteristic expression of cytokeratin]. *No To Shinkei*. 1990;42(7):675–682.
56. Xin W, Rubin MA, McKeever PE. Differential expression of cytokeratins 8 and 20 distinguishes craniopharyngioma from rathke cleft cyst. *Arch Pathol Lab Med*. 2002;126(10):1174–1178.
57. Apps JR, et al. Tumour compartment transcriptomics demonstrates the activation of inflammatory and odontogenic programmes in human adamantinomatous craniopharyngioma and identifies the MAPK/ERK pathway as a novel therapeutic target. *Acta Neuropathol*. 2018;135(5):757–777.
58. Jucá CEB, et al. Impact of the canonical Wnt pathway activation on the pathogenesis and prognosis of adamantinomatous craniopharyngiomas. *Horm Metab Res*. 2018;50(7):575–581.
59. Schweizer L, et al. BRAF V600E analysis for the differentiation of papillary craniopharyngiomas and Rathke's cleft cysts. *Neuropathol Appl Neurobiol*. 2015;41(6):733–742.
60. Coy S, et al. Distinct patterns of primary and motile cilia in Rathke's cleft cysts and craniopharyngioma subtypes. *Mod Pathol*. 2016;29(12):1446–1459.
61. Meyerholz DK, et al. Glycogen depletion can increase the specificity of mucin detection in airway tissues. *BMC Res Notes*. 2018;11(1):763.
62. Jullien N, et al. Heterozygous LHX3 mutations may lead to a mild phenotype of combined pituitary hormone deficiency. *Eur J Hum Genet*. 2019;27(2):216–225.
63. Zhao Y, Morales DC, Hermesz E, Lee WK, Pfaff SL, Westphal H. Reduced expression of the LIM-homeobox gene Lhx3 impairs growth and differentiation of Rathke's pouch and increases cell apoptosis during mouse pituitary development. *Mech Dev*. 2006;123(8):605–613.
64. Dasen JS, et al. Reciprocal interactions of Pit1 and GATA2 mediate signaling gradient-induced determination of pituitary cell types. *Cell*. 1999;97(5):587–598.
65. Gordon DF, et al. Pit-1 and GATA-2 interact and functionally cooperate to activate the thyrotropin beta-subunit promoter. *J Biol Chem*. 1997;272(39):24339–24347.
66. Lo A, Zheng W, Gong Y, Crochet JR, Halvorson LM. GATA transcription factors regulate LHβ gene expression. *J Mol Endocrinol*. 2011;47(1):45–58.
67. Ohba K, et al. GATA2 mediates thyrotropin-releasing hormone-induced transcriptional activation of the thyrotropin β gene. *PLoS ONE*. 2011;6(4):e18667.
68. Hayashi S, McMahon AP. Efficient recombination in diverse tissues by a tamoxifen-inducible form of Cre: a tool for temporally regulated gene activation/inactivation in the mouse. *Dev Biol*. 2002;244(2):305–318.
69. Kyrousi C, et al. Mcidas and GemC1 are key regulators for the generation of multiciliated ependymal cells in the adult neurogenic niche. *Development*. 2015;142(21):3661–3674.
70. Zaret KS, Carroll JS. Pioneer transcription factors: establishing competence for gene expression. *Genes Dev*. 2011;25(21):2227–2241.
71. Norquay LD, Yang X, Jin Y, Detillieux KA, Cattini PA. Hepatocyte nuclear factor-3alpha binding at P sequences of the human growth hormone locus is associated with pituitary repressor function. *Mol Endocrinol*. 2006;20(3):598–607.
72. Brinkmeier ML, et al. Discovery of transcriptional regulators and signaling pathways in the developing pituitary gland by bioinformatic and genomic approaches. *Genomics*. 2009;93(5):449–460.
73. Carreno G, et al. Hypothalamic sonic hedgehog is required for cell specification and proliferation of LHX3/LHX4 pituitary embryonic precursors. *Development*. 2017;144(18):3289–3302.
74. Charles et al. Pituitary-specific *Gata2* knockout: effects on gonadotrope and thyrotrope function. *Mol Endocrinol*. 2006;20(6):1366–1377.
75. Zhang Q, et al. Collaborative ISL1/GATA3 interaction in controlling neuroblastoma oncogenic pathways overlapping with but distinct from MYCN. *Theranostics*. 2019;9(4):986–1000.
76. Zada G, Lin N, Ojerholm E, Ramkissoon S, Laws ER. Craniopharyngioma and other cystic epithelial lesions of the sellar region: a review of clinical, imaging, and histopathological relationships. *Neurosurg Focus*. 2010;28(4):E4.
77. Gonzalez-Meljem JM, et al. Stem cell senescence drives age-attenuated induction of pituitary tumours in mouse models of paediatric craniopharyngioma. *Nat Commun*. 2017;8(1):1819.
78. Stache C, et al. Insights into the infiltrative behavior of adamantinomatous craniopharyngioma in a new xenotransplant mouse model. *Brain Pathol*. 2015;25(1):1–10.
79. Kaku Y, et al. Islet1 deletion causes kidney agenesis and hydroureter resembling CAKUT. *J Am Soc Nephrol*. 2013;24(8):1242–1249.
80. Liang X, et al. Transcription factor ISL1 is essential for pacemaker development and function. *J Clin Invest*. 2015;125(8):3256–3268.
81. Su T, et al. LIM homeodomain transcription factor Isl1 affects urethral epithelium differentiation and apoptosis via Shh. *Cell Death Dis*. 2019;10(10):713.
82. Zhang Q, et al. Temporal requirements for ISL1 in sympathetic neuron proliferation, differentiation, and diversification. *Cell Death Dis*. 2018;9(2):247.
83. Ellsworth BS, et al. FOXL2 in the pituitary: molecular, genetic, and developmental analysis. *Mol Endocrinol*. 2006;20(11):2796–2805.
84. Ingraham HA, et al. The nuclear receptor steroidogenic factor 1 acts at multiple levels of the reproductive axis. *Genes Dev*. 1994;8(19):2302–2312.
85. Tran S, et al. Impaired fertility and FSH synthesis in gonadotrope-specific Foxl2 knockout mice. *Mol Endocrinol*. 2013;27(3):407–421.
86. Granger A, Bleux C, Kottler ML, Rhodes SJ, Counis R, Laverrière JN. The LIM-homeodomain proteins Isl-1 and Lhx3 act with steroidogenic factor 1 to enhance gonadotrope-specific activity of the gonadotropin-releasing hormone receptor gene promoter. *Mol Endocrinol*. 2006;20(9):2093–2108.
87. Lu KM, Evans SM, Hirano S, Liu FC. Dual role for Islet-1 in promoting striatonigral and repressing striatopallidal genetic programs to specify striatonigral cell identity. *Proc Natl Acad Sci USA*. 2014;111(1):E168–E177.
88. Naveau A, et al. Isl1 controls patterning and mineralization of enamel in the continuously renewing mouse incisor. *J Bone Miner Res*. 2017;32(11):2219–2231.
89. Besnard V, Wert SE, Kaestner KH, Whitsett JA. Stage-specific regulation of respiratory epithelial cell differentiation by Foxa1. *Am J Physiol Lung Cell Mol Physiol*. 2005;289(5):L750–L759.
90. Chimelli L, et al. Intra-sellar salivary gland-like pleomorphic adenoma arising within the wall of a Rathke's cleft cyst. *Pituitary*. 2000;3(4):257–261.
91. Kusakabe M, Sakakura T, Sano M, Nishizuka Y. A pituitary-salivary mixed gland induced by tissue recombination of embryonic pituitary epithelium and embryonic submandibular gland mesenchyme in mice. *Dev Biol*. 1985;110(2):382–391.
92. Ranucci V, et al. Ectopic salivary gland tissue in a Rathke's cleft cyst. *Int J Clin Exp Pathol*. 2013;6(7):1437–1440.
93. Wan H, et al. Compensatory roles of Foxa1 and Foxa2 during lung morphogenesis. *J Biol Chem*. 2005;280(14):13809–13816.
94. Tompkins DH, et al. Sox2 activates cell proliferation and differentiation in the respiratory epithelium. *Am J Respir Cell Mol Biol*. 2011;45(1):101–110.
95. Ochieng JK, et al. Sox2 regulates the emergence of lung basal cells by directly activating the transcription of Trp63. *Am J Respir Cell Mol Biol*. 2014;51(2):311–322.
96. Rockich BE, et al. Sox9 plays multiple roles in the lung epithelium during branching morphogenesis. *Proc Natl Acad Sci USA*. 2013;110(47):E4456–E4464.
97. Home P, et al. Genetic redundancy of GATA factors in the extraembryonic trophoblast lineage ensures the progression of preimplantation and postimplantation mammalian development. *Development*. 2017;144(5):876–888.
98. Hoshino T, et al. Spiral ganglion cell degeneration-induced deafness as a consequence of reduced GATA factor activity. *Genes Cells*. 2019;24(8):534–545.
99. Kouros-Mehr H, Slorach EM, Sternlicht MD, Werb Z. GATA-3 maintains the differentiation of the luminal cell fate in the mammary gland. *Cell*. 2006;127(5):1041–1055.
100. Bielmeier C, et al. Interface contractility between differently fated cells drives cell elimination and cyst formation. *Curr Biol*. 2016;26(5):563–574.
101. Edgar R, Domrachev M, Lash AE. Gene Expression Omnibus: NCBI gene expression and hybridization array data repository. *Nucleic Acids Res*. 2002;30(1):207–210.